

Accounting for data heterogeneity in integrative analysis and prediction methods: An application to Chronic Obstructive Pulmonary Disease

J. Butts¹, C. Wendt², R. Bowler³, C.P. Hersh⁴, Q. Long⁵, L. Eberly¹, and S. E. Safo^{1*}

¹Division of Biostatistics, University of Minnesota, Minneapolis, MN, USA,

²Division of Pulmonary, Allergy and Critical Care
University of Minnesota, Minneapolis, MN, USA

³Division of Pulmonary, Critical Care and Sleep Medicine

Department of Medicine, National Jewish Health, Denver, CO, USA and

⁴Channing Division of Network Medicine, Brigham and Women's Hospital
Harvard Medical School, Boston, MA, USA

⁵ Department of Biostatistics, Epidemiology and Informatics
Perelman School of Medicine, University of Pennsylvania
Philadelphia, PA, USA

**Corresponding author: ssafo@umn.edu*

November 16, 2021

Abstract

Epidemiologic and genetic studies in chronic obstructive pulmonary disease (COPD) and many complex diseases suggest subgroup disparities (e.g., by sex). We consider this problem from the standpoint of integrative analysis where we combine information from different views (e.g., genomics, proteomics, clinical data). Existing integrative analysis methods ignore the heterogeneity in subgroups, and stacking the views and accounting for subgroup heterogeneity does not model the association among the views. To address analytical challenges in the problem of our interest, we propose a statistical approach for joint association and prediction that leverages the strengths in each view to identify molecular signatures that are shared by and specific to males and females and that contribute to the variation in COPD, measured by airway wall thickness. HIP (Heterogeneity in Integration and Prediction) accounts for subgroup heterogeneity, allows for sparsity in variable selection, is applicable to multi-class and to univariate or multivariate continuous outcomes, and incorporates covariate adjustment. We develop efficient algorithms in PyTorch. Our COPD findings have identified several proteins, genes, and pathways that are common and specific to males and females, some of which have been implicated in COPD, while others could lead to new insights into sex differences in COPD mechanisms.

Keywords: COPD; Multi-view data; Multi-view learning; One-step methods; Subgroup heterogeneity.

1 Introduction

Chronic obstructive pulmonary disease (COPD) is a chronic progressive disease affecting more than 16 million adults, presenting a substantial and increasing economic and social burden (Wheaton et al., 2015); COPD was projected to cost the U.S. economy about \$49 billion in 2020 (Guarascio et al., 2013). Although tobacco smoking is the leading environmental risk factor for COPD, even in heavy smokers fewer than 50% develop COPD (GOLD, 2020). The Genetic Epidemiology of COPD (COPDGene) Study (Regan et al., 2011) is one of the largest studies to investigate the underlying genetic factors of COPD to understand why certain smokers develop COPD while others do not. While many genomic studies have successfully identified multiple genetic variants for COPD susceptibility, most identified genetic variants do not reside in protein-coding regions (Silverman, 2018) making it difficult to interpret their function. Genomics data used in combination with other omics (e.g., proteomics) and known risk factors show promise in identifying multifaceted features that can enhance our understanding of mechanisms of COPD susceptibility.

Epidemiologic and genetic studies suggest subgroup (e.g., sex) disparities exist for many complex diseases. Subgroups of a population can present similar symptoms but have different clinical courses and respond to therapy differently. By determining factors predictive of an outcome for each subgroup, we can better personalize treatments to improve patient outcomes. Research suggests sex disparities exist in COPD mechanisms (Barnes, 2016). A meta-analysis review of 11 studies showed that female smokers, even if smoking fewer cigarettes, had a faster annual decline in forced expiratory volume in one second (FEV_1) (Gan et al., 2006). A study using COPDGene data found women smokers tended to have higher airway wall thickness (AWT) compared to male smokers (Kim et al., 2011), likely explaining some of the sex differences in the prevalence of COPD. Women with severe COPD may be at higher risk for hospitalization and death (Prescott et al., 1997). These studies primarily used data from one source, so combining data from multiple sources has the potential to reveal new insights into sex differences in COPD mechanisms. Motivated by the crucial scientific need to understand sex differences in COPD, we leverage the strengths from multiple data views from the COPDGene Study (Regan et al., 2011) to identify and explore genes and proteins *common* and *specific* to males and females that contribute to variation in AWT.

Existing methods for integrating data from multiple views are inadequate for our problem as they do not account for subgroup heterogeneity. In particular, one-step methods have been proposed for joint association of data from multiple views and simultaneous prediction of an outcome (Safo et al., 2021; Chekouo and Safo, 2020; Luo et al., 2016) that potentially could be used. To do this, one would build a separate model for each subgroup and then determine the important multidimensional variables that are associated and predictive of the outcome for each subgroup. While this approach is intuitive, it is limited by the sample size for each subgroup and does not pool information across subgroups making estimation challenging. This is especially true for high-dimensional data settings where the number of variables is larger than the sample size for each subgroup. Another approach that makes use of samples in all subgroups is to apply these one-step methods on the combined subgroup data, but this precludes us from examining whether such heterogeneity exists.

The need to account for subgroup heterogeneity has been recognized and studied in the case where there is only one data view. Dondelinger et al. (2018) propose the Joint Lasso to jointly estimate regression coefficients for different subgroups while allowing for

the identification of subgroup-specific features, and also encouraging similarity between subgroup-specific coefficients. In Li et al. (2014), the authors proposed a lasso method for feature selection for different studies (in our application, subgroups) that incorporates a hierarchical penalty to borrow strength across different studies, while allowing for feature selection flexibility. To use these existing methods, one would stack the different data views for each subgroup; this approach assumes the many variables across the data views are independent and ignores the overall dependency structure among the different views.

In this article, we consider integrative analysis and prediction methods that account for subgroup heterogeneity and are appropriate for our motivating data. We consider a modified version of the hierarchical penalty proposed in Li et al. (2014) to improve power for selecting common and subgroup-specific features. The methods we propose, called HIP (Heterogeneity in Integration and Prediction), are applicable to multi-class and continuous outcomes, allow for multiple continuous outcomes, and can force specified covariates into the model. We develop computationally efficient algorithms in PyTorch. We apply the methods to our motivating data from the COPDGene Study to identify genes and proteins common and specific to males and females and associated with AWT. We also explore the utility of these omics biomarkers in predicting AWT beyond established COPD risk factors.

2 Methods

2.1 Notation and Problem

Suppose we have D views (e.g., genomics, proteomics) with p_d variables measured on the same N subjects. Each view has $s = 1, \dots, S$ subgroups known a priori, each with sample size n_s where $N = \sum_{s=1}^S n_s$. For subgroup s and view d , $\mathbf{X}^{d,s} \in \mathbb{R}^{n_s \times p_d}$ represents the data matrix. Assume we also have outcome data for each subgroup. For a continuous outcome(s) (e.g., AWT), we have matrix $\mathbf{Y}^s \in \mathbb{R}^{n_s \times q}$ where q is the number of outcomes. For a multi-class outcome with m unique classes, let $\mathbf{Y}^s \in \mathbb{R}^{n_s \times m}$ be an indicator matrix with the ij th entry being 1 if sample i in subgroup s belongs to class j , and 0 otherwise. Our primary goal is to perform integrative analysis that considers the overall dependency structure among views, predicts an outcome, incorporates feature selection, and accounts for subgroup heterogeneity to identify common and subgroup-specific variables contributing to variation in the outcome.

2.2 Integration of omics and clinical data

To relate the omics and/or clinical data for each subgroup, we assume there are common unobserved scores for each subgroup (\mathbf{Z}^s) that drive the dependency structure among the different views. Then, each view is written as the product of the common scores $\mathbf{Z}^s \in \mathbb{R}^{n_s \times K}$ and a matrix of view-specific factor loadings $\mathbf{B}^{d,s} \in \mathbb{R}^{p_d \times K}$ plus a matrix of errors: $\mathbf{X}^{d,s} = \mathbf{Z}^s \mathbf{B}^{d,sT} + \mathbf{E}^{d,s}$. Here, $k = 1, \dots, K$ is the number of latent components used to approximate each view, and \mathbf{Z}^s connects the D views for subgroup s . The unobserved common scores explain the correlation across views for subgroup s , and $\mathbf{E}^{d,s}$ explains the remaining variability unique to each view for subgroup s .

We can consider $\mathbf{Z}^s \mathbf{B}^{d,sT}$ to approximate $\mathbf{X}^{d,s}$. We can then solve for $\mathbf{Z}^s \mathbf{B}^{d,sT}$ by minimizing the error, $\mathbf{E}^{d,s}$, via the loss function $F(\mathbf{X}^{d,s}, \mathbf{Z}^s, \mathbf{B}^{d,s}) = \|\mathbf{X}^{d,s} - \mathbf{Z}^s \mathbf{B}^{d,sT}\|_F^2$.

For a random matrix \mathbf{A} , $\|\mathbf{A}\|_F^2$ is the square of the Frobenius norm and is defined as $\text{trace}(\mathbf{A}^T \mathbf{A})$.

2.2.1 Hierarchical Penalty for Common and Subgroup-Specific Feature Selection

A main goal in this paper is to identify common and subgroup-specific omics features associated with an outcome. We use the hierarchical reparameterization proposed in Li et al. (2014) to decompose $\mathbf{B}^{d,s}$ as the element-wise product of \mathbf{G}^d and $\mathbf{\Xi}^{d,s}$ i.e., $\mathbf{B}^{d,s} = \mathbf{G}^d \cdot \mathbf{\Xi}^{d,s}$ for $d = 1, \dots, D$ and $s = 1, \dots, S$ to estimate effects that are common across subgroups using $\mathbf{G}^d \in \mathfrak{R}^{p_d \times K}$ while also allowing for heterogeneity in the subgroups through $\mathbf{\Xi}^{d,s} \in \mathfrak{R}^{p_d \times K}$. If there is no heterogeneity, then $\mathbf{\Xi}^{d,s}$ is a matrix of ones for all s , and $\mathbf{G}^d = \mathbf{B}^d$, i.e., the data-specific loadings for each view are the same for each subgroup. In estimating \mathbf{G}^d , we borrow strength across subgroups for increased power.

We use regularization to induce sparsity by adding the block l_1/l_2 penalty on \mathbf{G}^d and $\mathbf{\Xi}^{d,s}$:

$$\sum_{s=1}^S \mathcal{J}(\mathbf{B}^{d,s}) = \lambda_G \gamma_d \sum_{l=1}^{p_d} \|\mathbf{g}_l^d\|_2 + \lambda_\xi \gamma_d \sum_{s=1}^S \sum_{l=1}^{p_d} \|\boldsymbol{\xi}_l^{d,s}\|_2. \quad (1)$$

Here, \mathbf{g}_l^d and $\boldsymbol{\xi}_l^{d,s}$ are the l th rows in \mathbf{G}^d and $\mathbf{\Xi}^{d,s}$ respectively and are each length K . By imposing the block l_1/l_2 penalty on the rows of \mathbf{G}^d and $\mathbf{\Xi}^{d,s}$, the $k = 1, \dots, K$ latent components are considered as a group encouraging variables to be selected in all K components or not to be selected. This differs from the original hierarchical penalty reparameterization proposed in Li et al. (2014) which imposes an l_1 penalty.

Both λ_G and λ_ξ are tuning parameters controlling feature selection. Specifically, λ_G controls feature selection for all subgroups combined and encourages removal of variables that are not important for all S subgroups. Also, λ_ξ encourages feature selection for each subgroup. Further details on the selection of λ_G and λ_ξ are given in Section 3.3. The γ_d parameter is an indicator for whether the view should be penalized. This is to allow some views, such as a set of clinical covariates, to be forced into the model as using clinical covariates to guide the selection of other important variables can result in better prediction of the outcome.

2.3 Relating Common Factors to Clinical Outcome(s)

Our end goal is to be able to make a prediction on the outcome that allows for heterogeneity in effects based on the subgroup and multi-view data. As such, we assume the outcome is related to the views only through the common scores for each subgroup. This allows us to couple the problem of associating the different views and predicting an outcome. We relate the outcome to \mathbf{Z}^s by minimizing a loss function $\sum_{s=1}^S F(\mathbf{Y}^s, \mathbf{Z}^s, \boldsymbol{\Theta})$ which depends on the type of outcome. For continuous outcome(s), $F(\mathbf{Y}^s, \mathbf{Z}^s, \boldsymbol{\theta}) = \|\mathbf{Y}^s - \mathbf{Z}^s \boldsymbol{\theta}\|_F^2$, where $\boldsymbol{\Theta} \in \mathfrak{R}^{K \times q}$ are regression coefficients. Here, we assume each column of \mathbf{Y}^s has been standardized to have mean 0 and variance 1 at the subgroup level. For a multi-class outcome, we consider the cross-entropy loss function $F(\mathbf{Y}^s, \mathbf{Z}^s, \boldsymbol{\Theta}) = -\sum_{i=1}^{n_s} \sum_{j=1}^m y_{ij}^s \log(a_{ij}^s)$ where $a_{ij}^s = \frac{\exp\{w_{ij}^s\}}{\sum_{j=1}^m \exp\{w_{ij}^s\}}$ is the *softmax* function generalizing logistic regression from binary to multi-class problems. Here, $\mathbf{W}^s = \mathbf{Z}^s \boldsymbol{\Theta} \in \mathfrak{R}^{n_s \times m}$ represents scores, $\boldsymbol{\Theta} \in \mathfrak{R}^{K \times m}$ represents weights corresponding to scores, and w_{ij}^s is the ij th entry in \mathbf{W}^s . The softmax function

applies the exponential function to each w_{ij}^s , and normalizes by the sum of these exponentials so the sum of each row in \mathbf{W}^s is 1, and each normalized entry represents a probability of belonging to class m . We note that Θ is common and not subgroup dependent. This allows the outcome data for all subgroups to be used when estimating these parameters and can improve the overall prediction of the outcome. Our proposal to model multiple continuous outcomes in a one-step integrative analysis model is novel and will be of use in many scientific applications.

2.4 Joint Model for Integration and Prediction

Our goal in using HIP (Heterogeneity in Integration and Prediction) is to estimate the following parameters: data-specific components $\mathbf{B}^{d,s}$ (\mathbf{G}^d , the common variables, and $\Xi^{d,s}$, the subgroup-specific variables), the shared latent scores for each subgroup (\mathbf{Z}^s), and the regression estimates (Θ). To obtain these estimates, we solve the following optimization:

$$(\widehat{\mathbf{B}}^{d,s}, \widehat{\mathbf{Z}}^s, \widehat{\Theta}) = \min_{\mathbf{B}^{d,s}, \mathbf{Z}^s, \Theta} \sum_{s=1}^S F(\mathbf{Y}^s, \mathbf{Z}^s, \Theta) + \sum_{d=1}^D \sum_{s=1}^S F(\mathbf{X}^{d,s}, \mathbf{Z}^s, \mathbf{B}^{d,s}) + \sum_{d=1}^D \sum_{s=1}^S \mathcal{J}(\mathbf{B}^{d,s}). \quad (2)$$

Although the hierarchical penalty has been used before, our paper is among the first to use this penalty in joint association and prediction studies for data from multiple views to account for common and subgroup-specific variation and to extract subgroup-specific omics and/or clinical variables. In Section 3, we describe our algorithm for obtaining these estimates.

2.5 Prediction

In order to predict an outcome on new data (say $\mathbf{X}_{test}^{d,s}$), we first predict the test shared component, \mathbf{Z}_{pred}^s , and then use this information to predict the outcome. To predict \mathbf{Z}_{pred}^s , we learn the model on the training data (i.e., $\mathbf{X}^{d,s}$), obtain the learned estimates $\widehat{\mathbf{B}}^{d,s}$ and $\widehat{\theta}$ or $\widehat{\Theta}$, and given these estimates and the testing data $\mathbf{X}_{test}^{d,s}$, we solve the problem:

$$\widehat{\mathbf{Z}}_{pred}^s = \min_{\mathbf{Z}^s} \sum_{d=1}^D \sum_{s=1}^S F(\mathbf{X}_{test}^{d,s}, \mathbf{Z}^s, \widehat{\mathbf{B}}^{d,s}) = \min_{\mathbf{Z}^s} \sum_{d=1}^D \sum_{s=1}^S \|\mathbf{X}_{test}^{d,s} - \mathbf{Z}^s \widehat{\mathbf{B}}^{d,s^T}\|_F^2.$$

The solution of this problem has a closed form which is given by $\widehat{\mathbf{Z}}_{pred}^s = \mathbf{X}_{cat}^s \widehat{\mathbf{B}}_{cat}^s (\widehat{\mathbf{B}}_{cat}^{s^T} \widehat{\mathbf{B}}_{cat}^s)^{-1}$ for $s = 1, \dots, S$. Here, \mathbf{X}_{cat}^s is an $n_s \times \{p_1 + \dots + p_D\}$ matrix that concatenates all D views for subgroup s , i.e., $\mathbf{X}_{cat}^s = [\mathbf{X}_{test}^{1,s}, \dots, \mathbf{X}_{test}^{D,s}]$. Similarly, $\widehat{\mathbf{B}}_{cat}^s = [\widehat{\mathbf{B}}^{1,s}, \dots, \widehat{\mathbf{B}}^{D,s}]$ and is a $\{p_1 + \dots + p_D\} \times K$ matrix of variable coefficients. We add a small multiple of the identity matrix before taking the inverse to help with stability. Note that we take an inverse of a $K \times K$ matrix, which is computationally inexpensive since K is typically a small number. Once we have obtained $\widehat{\mathbf{Z}}_{pred}^s$, we predict a continuous outcome $\widehat{\mathbf{Y}}_{pred}^s$ as $\widehat{\mathbf{Y}}_{pred}^s = \widehat{\mathbf{Z}}_{pred}^s \widehat{\Theta}$. For a multi-class outcome, we obtain the predicted class probabilities as $\widehat{a}_{ij_{pred}}^s = \frac{\exp\{\widehat{w}_{ij}^s\}}{\sum_{j=1}^m \exp\{\widehat{w}_{ij}^s\}}$, where \widehat{w}_{ij}^s is the ij th entry in $\widehat{\mathbf{W}}^s = \widehat{\mathbf{Z}}_{pred}^s \widehat{\Theta}$. Given the predicted class probabilities, we obtain the predicted class membership for sample i as $\widehat{y}_{i_{pred}}^s = \arg \max_j \widehat{a}_{ij_{pred}}^s$.

3 Algorithm

3.1 Initializations

To initialize $\mathbf{Z}^{s(0)}$, we first obtain the left singular vectors from the singular value decomposition of the concatenated data matrix for subgroup $s, s = 1, \dots, S$ across $d = 1, \dots, D$ (i.e., all data combined). Then we set $\mathbf{Z}^{1(0)}$ as the first $n_1 \times K$ entries in the left singular vectors, $\mathbf{Z}^{2(0)}$ is the next $n_2 \times K$ entries, and so on. We initialize both $\mathbf{G}^{d(0)}$ and $\Xi^{d,s(0)}$ as a $p_d \times K$ matrix of ones. To initialize Θ in the continuous case, we regress the scaled \mathbf{Y} on the first K columns of the SVD of the full concatenated data matrix. In the multi-class case, the $n \times m$ matrix Θ is initialized with random numbers from a $U(0, 1)$ distribution. In both cases, the columns are normalized to have unit length.

3.2 Optimization

The optimization problem in (2) is multi-convex in $\mathbf{B}^{d,s}, \mathbf{Z}^s$ and Θ each but jointly non-convex. As such, we are not guaranteed convergence to a global minimum. A local optimum can be found by iteratively minimizing over each of the optimization parameters with the rest of the optimization parameters fixed. Convergence is determined by the change in the objective function in (2) without the penalty terms.

3.2.1 Estimate $\Xi^{d,s}$

In order to estimate $\Xi^{d,s(t+1)}$, we fix \mathbf{Z}^s and \mathbf{G}^d at their values in iteration $t, t \geq 0$ and solve $\widehat{\Xi}^{d,s(t+1)} = \min_{\Xi^{d,s} \in \mathbb{R}^{p_d \times K}} \|(\mathbf{X}^{d,s} - \mathbf{Z}^{s(t)}(\mathbf{G}^{d(t)} \cdot \Xi^{d,s})^T)\|_F^2 + \lambda_\xi \gamma_d \sum_{l=1}^{p_d} \|\xi_l^{d,s}\|_2$. We optimize differently depending on whether the view is penalized. Without penalization, $\Xi^{d,s(t+1)}$ is estimated by the Adagrad optimizer (Duchi et al., 2011) implemented in the PyTorch package (Paszke et al., 2019). The Adagrad optimizer is a gradient descent algorithm that adapts the learning rate to the frequency of the features associated with each parameter (Ruder, 2016). Convergence is determined by the relative change in the objective function defined above being less than ϵ . With penalization, we use an accelerated projected gradient descent algorithm sped up with FISTA (Beck and Teboulle, 2009). FISTA accomplishes improved speed by using a linear combination of the previous two iteration estimates when updating optimization parameters rather than just the previous iteration estimates (Beck and Teboulle, 2009). Since our regularization penalty is the block l_2/l_1 penalty, we implement the l_2/l_1 projection proposed in (Liu et al., 2009) during the projection step in FISTA. We set the convergence criterion as $\frac{\|\Xi^{d,s(t+1)} - \Xi^{d,s(t)}\|_F^2}{p_d} < \epsilon$.

3.2.2 Estimate \mathbf{G}^d

Once we have estimated $\Xi^{d,s}$ at the $(t+1)$ th iteration, we use this estimate to find $\mathbf{G}^{d(t+1)}$ by solving $\widehat{\mathbf{G}}^{d(t+1)} = \min_{\mathbf{G}^d \in \mathbb{R}^{p_d \times K}} \sum_{s=1}^S \|(\mathbf{X}^{d,s} - \mathbf{Z}^{s(t)}(\mathbf{G}^d \cdot \Xi^{d,s(t+1)})^T)\|_F^2 + \lambda_G \gamma_d \sum_{l=1}^{p_d} \|\mathbf{g}_l^d\|_2$. Without penalization, we use the same Adagrad optimizer implemented in PyTorch as was employed in the $\Xi^{d,s}$ optimization. Convergence is determined by the relative change in the objective function being less than ϵ . With penalization, we again use projected gradient descent with FISTA acceleration, and we implement the projection from Liu et al. (2009). The convergence criterion is $\frac{\|\mathbf{G}^{d(t+1)} - \mathbf{G}^{d(t)}\|_F^2}{p_d} < \epsilon$.

3.2.3 Estimate \mathbf{Z}^s

With the estimates $\hat{\Xi}^{d,s(t+1)}$ and $\hat{\mathbf{G}}^{d(t+1)}$, we obtain $\mathbf{B}^{d,s(t+1)}$ and we use this to estimate $\mathbf{Z}^{s(t+1)}$ by optimizing

$$\hat{\mathbf{Z}}^{s(t+1)} = \min_{\mathbf{Z}^s} \sum_{s=1}^S F(\mathbf{Y}^s, \mathbf{Z}^s, \Theta^{(t)}) + \sum_{d=1}^D \sum_{s=1}^S \|\mathbf{X}^{d,s} - \mathbf{Z}^s \mathbf{B}^{d,s(t+1)T}\|_F^2. \quad (3)$$

For continuous outcome(s), there is a closed form solution. Both the association and prediction terms of the optimization include \mathbf{Z}^s in a squared Frobenius norm, so we combine these two losses into one loss. Let $\tilde{\mathbf{X}}^s = [\mathbf{X}^{1,s} \dots \mathbf{X}^{D,s}, \mathbf{Y}^s]$ be an $\{n_s \times (p_1 + \dots + p_D + q)\}$ matrix concatenating the views and outcome(s), and let $\tilde{\mathbf{B}}^s = [\mathbf{B}^{1,sT} \dots \mathbf{B}^{D,sT} \Theta]$ be a $\{K \times (p_1 + \dots + p_D + q)\}$ matrix of coefficients (where we have suppressed the superscripts $(t+1)$ in $\mathbf{B}^{d,s(t+1)}$ and (t) in $\Theta^{(t)}$). Then equation (3) reduces to $\|\tilde{\mathbf{X}}^s - \mathbf{Z}^s \tilde{\mathbf{B}}^s\|_F^2$, which can be rewritten as $\|\tilde{\mathbf{X}}^{sT} - \tilde{\mathbf{B}}^{sT} \mathbf{Z}^{sT}\|_F^2$. This is a standard least squares problem with the solution given as $\mathbf{Z}^{sT} = (\tilde{\mathbf{B}}^s \tilde{\mathbf{B}}^{sT})^{-1} \tilde{\mathbf{B}}^s \tilde{\mathbf{X}}^{sT}$. In the multi-class case, there is no closed form solution. We use a gradient descent algorithm implemented in the Adagrad optimizer (Duchi et al., 2011) in PyTorch (Paszke et al., 2019).

3.2.4 Estimate Θ

The final step is to solve for Θ using estimated \mathbf{Z}^s at the $(t+1)$ th iteration. The solution depends on the type of outcome. For a continuous outcome(s), it is a least squares regression problem with the closed form solution $\hat{\Theta}^{(t+1)} = (\mathbf{Z}^{(t+1)T} \mathbf{Z}^{(t+1)})^{-1} \mathbf{Z}^{(t+1)T} \mathbf{Y}$ where \mathbf{Z} and \mathbf{Y} are stacked so all subgroups are combined in each matrix. In the multi-class case, there is no closed form solution, so we can use any gradient descent algorithm to solve $\hat{\Theta}^{(t+1)} = \min_{\Theta} \sum_{s=1}^S F(\mathbf{Y}^s, \mathbf{Z}^{s(t+1)}, \Theta)$. We again choose to use the Adagrad optimizer (Duchi et al., 2011) as implemented in PyTorch (Paszke et al., 2019).

3.3 λ and K Selection

The optimization problem in equation (2) depends on tuning parameters $\lambda = (\lambda_G, \lambda_\xi)$. Ideally, one would search over the entire grid space, but this is computationally expensive. Instead, we use ideas in Bergstra and Bengio (2012) and randomly select grid values from the hyperparameter space to search over. Please refer to supporting material for more details. In order to select a set of λ values, we calculate the Bayesian Information Criterion (BIC) for a given λ : $BIC = -2 \left(\sum_{s=1}^S F(\mathbf{Y}^s, \mathbf{Z}^s, \Theta) + \sum_{d=1}^D \sum_{s=1}^S \|\mathbf{X}^{d,s} - \mathbf{Z}^s \mathbf{B}^{d,sT}\|_F^2 \right) + \lambda_B \log(N)$, and we choose the $\lambda = (\lambda_G, \lambda_\xi)$ combination that results in the smallest BIC. Here, λ_B is the sum of the number of non-zero rows across each of the $\mathbf{B}^{d,s}$ matrices.

We propose two automatic ways for selecting the number of components, K . Please refer to supporting material. We performed sensitivity analyses to determine how the results of the simulations would change based on K and found the results to be robust though computation time increased with the value of K (Web Figures 1-2).

4 Simulations

4.1 Set-up

Two simulation examples were examined: a continuous and a binary outcome. For all simulations, we used two views and two subgroups i.e., $D = S = 2$. There were $n_1 = 250$ subjects in the first subgroup and $n_2 = 260$ subjects in the second. There were two different scenarios to test the ability of the algorithm to perform variable selection and prediction: Full Overlap and Partial Overlap. These are described in Section 4.2 and depicted in Web Figure 3. For each example and scenario, there were three different numbers of variables in the data sets. In the P1 setting, the first data set had $p_1 = 300$ variables, and the second had $p_2 = 350$. In the P2 setting the first data set had $p_1 = 1,000$ variables, and the second had $p_2 = 1,500$. Finally, in the P3 setting, the first data set had $p_1 = 5,000$ variables, and the second had $p_2 = 6,000$. For these simulations, K was fixed to the true value of 2. We also conducted simulations to explore the ability of the algorithm to select K where we ran the simple and the algorithmic approaches for the Full and Partial P1 and P3 settings (Web Table 1).

The data generation process is based on Luo et al. (2016). First, the $\mathbf{B}^{d,s}$ matrices are generated according to the scenarios in Section 4.2. If the entry corresponds to an important variable, it is drawn from a $U(0.5, 1)$; otherwise it is set to 0. Once the entries are generated, we orthogonalize the columns of each matrix. Next, the \mathbf{Z}^s and $\mathbf{E}^{d,s}$ matrices are generated with entries from a standard normal distribution. Then the data matrix for subgroup s in view d is generated as $\mathbf{X}^{d,s} = \mathbf{Z}^s \mathbf{B}^{d,s^T} + \sigma_x \mathbf{E}^{d,s}$. Finally we form the outcome based on the type. For the continuous case, $\mathbf{Y}^s = \mathbf{Z}^s \boldsymbol{\Theta} + \sigma_y \mathbf{E}^s$ where $\mathbf{E}^s \in R^{n_s \times 1}$ contains entries from a standard normal distribution and the true value of $\boldsymbol{\Theta} = [1, 0]^T$. The values of σ_x and σ_y are held constant at 0.2 and 0.5 respectively. For the multi-class case, we form $\mathbf{W}^s = \mathbf{Z}^s \boldsymbol{\Theta}$ where $\boldsymbol{\Theta} = \begin{bmatrix} 1 & 0.5 \\ 0.8 & 0.2 \end{bmatrix}$. We then estimate the predicted probabilities for subgroup s , \mathbf{A}^s where $a_{ij}^s = \frac{e^{w_{ij}^s}}{\sum_{j=1}^m e^{w_{ij}^s}}$. Then we obtain the class membership for subject i , subgroup s as $y_i^s = \arg \max_j a_{ij}^s$. We generated 20 training and 20 independent testing data sets.

4.2 Two Scenarios

4.2.1 Scenario 1: Full Overlap

In this first scenario, there was complete overlap in the important variables for each subgroup i.e., the first 50 variables of the $\mathbf{B}^{d,s}$ matrices were important for both subgroups. We expect that competing methods will perform relatively well in this scenario as there is no heterogeneity between subgroups.

4.2.2 Scenario 2: Partial Overlap

In the second scenario, there is partial overlap in the important variables. The first 50 variables are important for the first subgroup. Of these 50, the last 25 are also important to the second subgroup in addition to the 25 subsequent variables. We expect to see some deterioration in the ability of the comparison methods to select the appropriate variables due to the heterogeneity in the subgroups.

4.3 Comparison Methods

We will compare our proposed method (HIP) to methods that perform integration but do not account for heterogeneity, methods that account for heterogeneity but do not perform integration, and methods that neither perform integration nor account for heterogeneity. First, we compare our method to canonical variate regression (CVR) (Luo et al., 2016). This is a joint association and prediction method for multiple views (although existing code can only implement two views), but it does not account for subgroup heterogeneity. Thus, we implement the method in two ways: (1) all subgroups are concatenated in each view (Concatenated CVR) and (2) a separate model is fit for each subgroup (Subgroup CVR). We allow the tuning parameters to be selected by the default method in the R package *CVR* (Luo and Chen, 2017). Second, we compare our method to the Joint Lasso (Dondelinger et al., 2018) as implemented in the R package *fuser* (Dondelinger and Wilkinson, 2018). The Joint Lasso does not perform integrative analysis but does account for subgroup heterogeneity. There is no function for choosing the two tuning parameters in the R package, so we implemented a grid search over the range $[0, 1]$ with 8 steps for each parameter. We implement this method on the data stacked over views (Concatenated Joint Lasso), but because Joint Lasso allows for subgroups, we also apply the method on each view separately (Dataset Joint Lasso). Third, we compare our method to the Lasso (Tibshirani, 1994) implemented using both the concatenated and separate subgroup models (Concatenated Lasso and Subgroup Lasso respectively); we stack the two views in each case. The tuning parameter was selected using the *cv.glmnet* function from the R package *glmnet* (Friedman et al., 2010). Finally, we compare our method to the Elastic Net (Zou and Hastie, 2005). Similar to the Lasso, we implement on both the concatenated and separate subgroup models (Concatenated Elastic Net and Subgroup Elastic Net respectively), and we stack the two views in each case. We set $\alpha = 0.5$ and select the optimal tuning parameter using the *cv.glmnet* function from the R package *glmnet* (Friedman et al., 2010). We implemented each of these methods on the training data sets and predicted the outcome using the test data sets.

4.4 Evaluation Measures

We compare HIP to existing methods in terms of variable selection and prediction. For variable selection, we estimate the true positive rate (TPR), false positive rate (FPR), and F1 score. All are constrained to the range $[0, 1]$. Note $\text{TPR} = \frac{\text{True Positives}}{\text{True Positives} + \text{False Negatives}}$, and $\text{FPR} = \frac{\text{False Positives}}{\text{True Negatives} + \text{False Positives}}$. Also, $\text{F1} = \frac{\text{True Positives}}{\text{True Positives} + \frac{1}{2}(\text{False Positives} + \text{False Negatives})}$. Ideally, TPR and F1 are 1 and FPR is 0. For prediction, we estimated the test mean squared error (MSE) for continuous outcome and the classification accuracy for binary outcome. Smaller MSE and higher classification accuracy indicate better performance. We averaged results over our 20 test data sets.

4.5 Continuous Outcome Results

In the Full Overlap scenario, we compare HIP using grid and random search [HIP (Grid) and HIP (Random) respectively] and find similar results. This supports using a random search over a grid search as it is much faster computationally (Web Figure 5).

Next we compare HIP to CVR (Luo et al., 2016) which integrates multiple data views

but does not account for subgroup heterogeneity. Since the subgroups have the same important variables in this condition, we do not expect much difference between CVR and the proposed method. We notice that HIP has a TPR and F1 close to 1 and FPR close to 0. These are better for HIP than CVR though CVR is the closest existing method for F1 score. However, results from CVR show more variation in these measures. In terms of prediction accuracy, HIP has lower test MSEs. Results for CVR from the P3 method are not reported because of the infeasible computation time required to apply this method.

Then we compare HIP to the Joint Lasso (Dondelinger et al., 2018) which is not an integrative approach but does account for subgroup heterogeneity. For the Joint Lasso, the TPR is fairly high, but the FPR is also fairly high meaning it is selecting a lot of variables that are not important. Because of the high FPR, the F1 score is lower than the other methods. The Concatenated Joint Lasso has similar predictive accuracy as our method, but it does not perform variable selection nearly as well.

Finally, we compare HIP to the Lasso (Tibshirani, 1994) and Elastic Net (Zou and Hastie, 2005), neither of which take an integrative approach nor account for subgroup heterogeneity. Since the subgroups share important variables, the concatenated approach performs better than the subgroup approach as it has a larger sample size and thus more power to detect effects. We notice that the Lasso and Elastic Net have a lower TPR suggesting that these methods are missing important variables. The FPR is similar to HIP but is more variable in the P1 and P2 scenarios. Because of the lower TPR, the F1 score is also lower for the Lasso and Elastic Net compared to HIP. In terms of prediction, HIP has lower MSEs compared to Lasso and Elastic Net. Even when subgroups share the same set of important variables, we see the advantages of taking an integrative approach and accounting for heterogeneity. These results are consistent across all three settings. Details on computation time are in Web Figure 5. The results from the Partial Overlap scenario are similar to the Full Overlap scenario (Web Figure 4).

4.6 Binary Outcome Results

The binary outcome results for the Full Overlap scenario were similar to the results from the continuous outcome (Web Figure 6). The binary Partial Overlap scenario results also mirror the continuous results (Web Figure 7). Computation times are shown in Web Figures 8-9.

5 Real Data Analysis

5.1 Study Goals

As mentioned in the motivating data, sex disparities exist in COPD susceptibility. In this section, our goal is to use molecular data from the COPDGene Study (Regan et al., 2011) in combination with clinical data to gain new insights into the molecular architecture of COPD in males and females. We focus on individuals with COPD at Year 5 (defined as GOLD stage ≥ 1) who had proteomics, RNA-sequencing, and AWT data available at Year 5. Of the $N = 216$ individuals with COPD at Year 5 who had complete data, $n_1 = 124$ were males and $n_2 = 92$ were females. Table 1 gives some characteristics of subjects who had COPD at Year 5. We assessed for sex differences using t-tests for continuous variables and χ^2 tests for categorical variables. Subjects were predominantly non-Hispanic white,

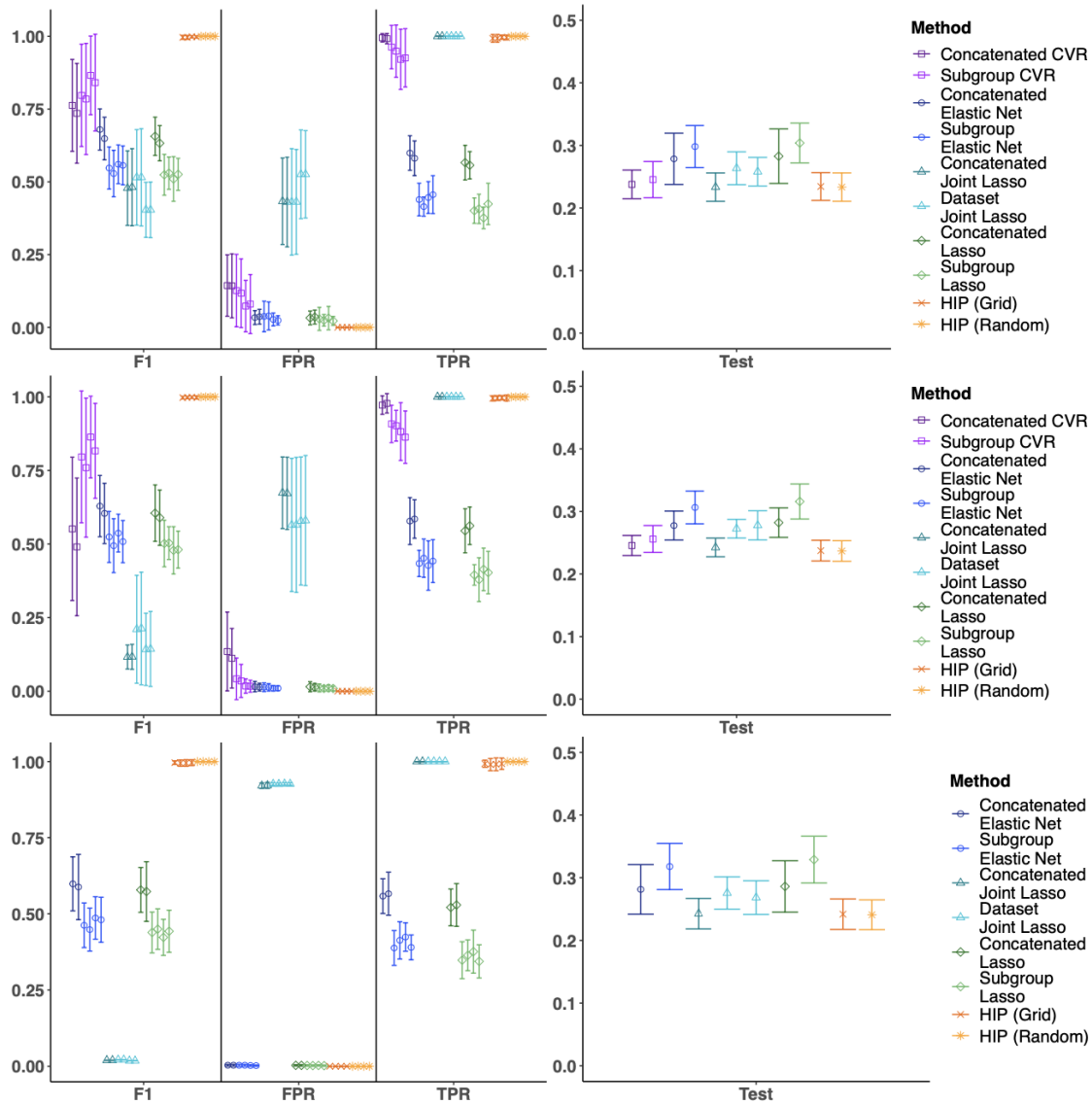


Figure 1: Results for Continuous Outcome, Full Overlap Scenario

The first row corresponds to P1 ($p_1 = 300$, $p_2 = 350$), the second to P2 ($p_1 = 1000$, $p_2 = 1500$), and the third to P3 ($p_1 = 5000$, $p_2 = 6000$). For all settings, $n_1 = 250$ and $n_2 = 260$. The right column is test mean squared error (MSE), so a lower value indicates better performance. All results are based on 20 iterations. Results for CVR are not reported for the P3 setting because the computational requirements render the model infeasible.

Table 1: Year 5 Characteristics of Participants with COPD

Variable	Male N=124	Female N=92	P-value
Age	71.31 (8.35)	68.78 (7.73)	0.023
BMI	28.63 (5.58)	27.26 (6.77)	0.117
FEV ₁ % Predicted	60.01 (21.94)	61.64 (24.60)	0.615
Change in FEV ₁ % Predicted	-3.40 (10.66)	-2.46 (9.78)	0.502
% Emphysema, Thirona	14.57 (13.15)	11.65 (12.28)	0.096
BODE Index	2.00 (1.97)	1.86 (1.79)	0.602
Pack Years of Smoking	55.10 (29.03)	46.23 (24.56)	0.016
Airway Wall Thickness	1.18 (0.23)	0.97 (0.21)	0.000
Non-Hispanic White (%)	95	93	0.815
Current Smoker (%)	15	27	0.049
Diabetes (%)	13	8	0.306

COPD = Chronic Obstructive Pulmonary Disease

BMI = Body Mass Index

FEV₁ = Forced Expiratory Volume in 1 Second

but there were no sex differences. Current smokers were more likely females. Male subjects tended to be older, had higher body mass index, and smoked more cigarettes. Males and females differed in their mean AWT ($p < 0.001$) but did not differ by lung function as measured by mean FEV₁% predicted. Given the available data, and the sex differences in AWT, we will i) identify genes and proteins common and specific to males and females and associated with AWT, ii) explore the pathways enriched in the proteins and genes identified for males and females, and iii) investigate the effect of these proteins and genes on AWT, adjusting for covariates.

5.2 Applying the proposed and competing methods

The original data set has 1,317 proteins and 21,669 RNAseq variables. To reduce dimensionality, we regressed each gene and protein with AWT and retained genes and proteins with potential to explain the variation in the outcome (p -value < 0.05). We had 297 proteins and 5,327 genes remaining. Our datasets for our analyses were: $\mathbf{X}^{1,1} \in \mathbb{R}^{124 \times 297}$, $\mathbf{X}^{2,1} \in \mathbb{R}^{124 \times 5,327}$, $\mathbf{Y}^1 \in \mathbb{R}^{124 \times 1}$ for males, and $\mathbf{X}^{1,2} \in \mathbb{R}^{92 \times 297}$, $\mathbf{X}^{2,2} \in \mathbb{R}^{92 \times 5,327}$, $\mathbf{Y}^2 \in \mathbb{R}^{92 \times 1}$ for females.

We used bootstrap resampling to identify stable molecules. We took 50 bootstrap samples from the original data to use as a training set while keeping the proportions of males and females, and the samples not selected in the training set became the test set. For each bootstrap training dataset, we applied HIP and existing methods. Elastic Net and Lasso do not account for subgroup heterogeneity and are applicable to only one data view. Thus, we stacked the views and we run separate analyses for males and females. Joint Lasso accounts for subgroup heterogeneity but is only applicable to one data view. Thus, we ran separate analyses for the protein and gene data. CVR is an integrative analysis method that does not account for subgroup heterogeneity so we ran separate analyses for males and females. We used both the random and grid searches to choose optimal tuning

parameters for HIP.

The comparison models were fit with the following R packages: *glmnet* (Friedman et al., 2010) for Lasso and Elastic Net, *CVR* (Luo and Chen, 2017) for CVR, and *fuser* (Dondelinger and Wilkinson, 2018) for Joint Lasso. To select tuning parameters, we minimized BIC for HIP, used 10-fold cross-validation for Lasso, Elastic Net, and CVR, and minimized test MSE for Joint Lasso. We set the tuning range of possible values for λ_G and λ_ξ in HIP to $(0, 3]$ since an upper bound of 1 resulted in loading matrices that were generally not sparse. Similarly, we used a grid search over $[0, 3]$ to select the two tuning parameters for the Joint Lasso. All other methods used default methods for selecting tuning parameters.

For HIP, the *simple* approach (threshold = 0.10) suggested $K = 6$ for the number of latent components, and the scree plot suggested $K = 4$ (Web Figure 10). Based on the robustness and computation times seen in the sensitivity analyses, we selected $K = 4$ components.

We then used the selected tuning parameters and bootstrap testing datasets to predict AWT and estimate test MSEs. We then selected the top 1% of genes and top 10% of proteins based on number of times selected in the bootstrap samples to represent the “stable” genes and proteins. Note that for the Joint Lasso, we set coefficients less than 10^{-7} in absolute value to 0; any variables whose coefficient was not set to 0 were considered to be selected.

5.3 Results

5.3.1 Average mean squared errors, and proteins and genes selected:

Web Table 6 shows the number of common and subgroup-specific genes and proteins identified by each method. We note few overlaps in selected genes and proteins between HIP and existing methods (Web Figure 12). Web Table 7 compares the variables selected by HIP (Random) and HIP (Grid). The average test MSEs from the bootstraps were slightly lower for Elastic Net and Lasso, but HIP had lower mean Test MSEs compared to CVR and Joint Lasso (Web Figure 11).

Web Tables 2-4 provide a list of the proteins and genes identified to be important to males and females by HIP (Random). We also report the weights for each protein and gene. We obtained $\hat{B}^{d,s}$, summed the absolute coefficients over the number of latent components, and averaged over the 50 bootstraps. Some proteins with large weights include MMP9, CADM1, ENG, and LY9 for males, and LY9 and ENG for females. The gene with the largest weight was CUL4A for both sexes. There is literature relating some of the proteins and genes identified to COPD. One study found MMP9 was a biomarker of increased acute exacerbations in patients with COPD in both the COPDGene and SPIROMICS (Subpopulations and Intermediate Outcome Measures in COPD Study) study populations (Wells et al., 2018). Another study found patients with COPD had increased CUL4A expression in small airway epithelium and CUL4A expression was inversely related to $FEV_1\%$ (Ren et al., 2019).

5.3.2 Gene Ontology Biological Processes and Pathway Enrichment Analysis

We used ToppGene Suite (Chen et al., 2009) to explore gene ontology (GO) biological processes that are enriched in the proteins and genes selected by HIP (Random) for males and females. The enriched GO terms for proteins included chemotaxis, taxis, cell adhesion, and biological adhesion. The enriched GO terms for genes included regulation of protein

localization to membrane and Golgi vesicle transport. There were some overlaps for males and females for our protein and gene lists as well as subgroup-specific GO terms (Web Table 5).

We also performed pathway enrichment analysis using Ingenuity Pathway Analysis (IPA) (Kramer et al., 2014) to test for overrepresentation of pathways among our list of proteins and genes for males and females. The Top 10 canonical protein pathways (Table 2) for males and females had some overlaps but also some subgroup-specific pathways. The top two pathways from the protein list for both sexes were osteoarthritis and airway inflammation in asthma. Previous research has shown asthma (particularly severe asthma) and COPD share some common inflammatory cells related to airway inflammation (Cukic et al., 2012). The top two pathways from the gene list for both sexes were regulation of actin-based motility by Rho and RhoA signaling. RhoA is part of a family of related proteins involved in cytoskeletal regulation including timing of cell division. Cigarette smoke impairs clearance of apoptotic cells through activation of RhoA in an animal model (Richens et al., 2009), and RhoA signaling has been associated with an emphysema phenotype (Qin et al., 2019).

5.3.3 Effect of common and sex-specific genes and proteins on AWT

Finally, we created common and sex-specific protein and gene scores from the proteins and genes selected by HIP (Random) and assessed whether these scores improved the prediction of AWT beyond some established COPD risk factors. We created the common protein score for subject i as $\text{CommonProtScore}_i = \sum_{j=1}^{\# \text{common proteins}} w_j x_{ij}^1$ where x_{ij}^1 is subject i 's protein expression value for the j th common protein (i.e., the ij th entry for the protein data, \mathbf{X}^1), and w_j is the weight for protein j . Each protein weight, w_j , was obtained via bootstrap. Specifically, we obtained 200 bootstrap datasets, and for each bootstrap dataset, we obtained regression coefficients and standard errors from univariate regression models of AWT and each of the common proteins identified. This resulted in 200 regression coefficients and standard errors which we combined using a weighted mean. The subgroup-specific scores were also obtained in a similar fashion. We also created opposite subgroup scores by using the protein/gene weights identified using the opposite subgroup; i.e. for a male subject, the opposite subgroup score is calculated using the weights calculated based on females and the proteins/genes identified to be important to females. The scores were standardized to have mean 0 and variance 1 in each subgroup since different variables were identified for males and females.

Once the scores were created, we fit several multiple linear regression models on the entire data: (1) Established Risk Factors (ERF) Model, (2) ERF + Common Protein Score, (3) ERF + Common Gene Score, (4) ERF + Common Protein and Gene Scores, (5) ERF + Subgroup Protein Score, (6) ERF + Subgroup Gene Score, (7) ERF + Subgroup Protein and Gene Scores. Table 3 shows the coefficient estimates with confidence intervals and p-values. We observe the scores, both common and subgroup-specific, are all statistically significant. The R^2 , which gives the amount of variation explained by the models, show that the models with the common scores and established risk factors were responsible for explaining at least 63.6% additional variation in AWT $[(0.229-0.140)/0.140]$ compared to the ERF model. The variation explained in AWT for the ERF + Subgroup Scores model was almost twice the variation explained in AWT by the ERF model.

We also compared how well the common and subgroup scores predicted AWT when

Table 2: Results for IPA Enrichment Analysis

View	Subgroup	Canonical Pathway	Molecules	Unadjusted P-value	
Proteins		Osteoarthritis Pathway	HMGB1,MMP9,S100A9,TNFRSF1B	0.037	
		Airway Inflammation in Asthma	ELANE,MMP9	0.054	
		Regulation Of The Epithelial Mesenchymal Transition By Growth Factors Pathway	MMP9,TNFRSF1B,TYK2	0.087	
		Axonal Guidance Signaling	MMP9,NTRK3,SEMA6A,SHH	0.121	
		PD-1, PD-L1 cancer immunotherapy pathway	TNFRSF1B,TYK2	0.147	
	Males	Neuroinflammation Signaling Pathway	HMGB1,MMP9,TYK2	0.153	
		Airway Pathology in Chronic Obstructive Pulmonary Disease	ELANE,MMP9	0.159	
		IL-15 Production	NTRK3,TYK2	0.167	
		LXR/RXR Activation	MMP9,TNFRSF1B	0.170	
		Pancreatic Adenocarcinoma Signaling	MMP9,TYK2	0.172	
	Genes		Osteoarthritis Pathway	HMGB1,MMP9,S100A9,TNFRSF1B	0.030
			Airway Inflammation in Asthma	ELANE,MMP9	0.049
			Axonal Guidance Signaling	MMP9,NTRK3,SEMA6A,SHH	0.099
			Airway Pathology in Chronic Obstructive Pulmonary Disease	ELANE,MMP9	0.144
			LXR/RXR Activation	MMP9,TNFRSF1B	0.153
Females		Role of IL-17A in Psoriasis	S100A9	0.183	
		Dermatan Sulfate Degradation (Metazoa)	IDS	0.188	
		HMGB1 Signaling	HMGB1,TNFRSF1B	0.188	
		Human Embryonic Stem Cell Pluripotency	INHBA,NTRK3	0.194	
		Granulocyte Adhesion and Diapedesis	MMP9,TNFRSF1B	0.204	
			Regulation of Actin-based Motility by Rho	ARPC2,ARPC3,MPRIP,PIP4K2A,RHOF	0.009
			RhoA Signaling	ARRGFEF12,ARPC2,ARPC3,MPRIIP,PIP4K2A	0.012
			Actin Cytoskeleton Signaling	ARRGFEF12,ARPC2,ARPC3,CRKL,DIAPH1,MPRIIP	0.018
			Integrin Signaling	ARPC2,ARPC3,CRKL,MPRIIP,RHOF	0.034
			RhoGDI Signaling	ARRGFEF12,ARPC2,ARPC3,PIP4K2A,RHOF	0.036
	Males	Reelin Signaling in Neurons	ARRGFEF12,ARPC2,ARPC3,CRKL	0.039	
		Signaling by Rho Family GTPases	ARRGFEF12,ARPC2,ARPC3,PIP4K2A,RHOF	0.056	
		Actin Nucleation by ARP-WASP Complex	ARPC2,ARPC3,RHOF	0.077	
		Coronavirus Replication Pathway	ARCNI,COPA	0.118	
		Rac Signaling	ARPC2,ARPC3,PIP4K2A	0.126	
			Regulation of Actin-based Motility by Rho	ARPC2,ARPC3,MPRIP,PIP4K2A,RHOF	0.008
			RhoA Signaling	ARRGFEF12,ARPC2,ARPC3,MPRIIP,PIP4K2A	0.009
			RhoGDI Signaling	ARRGFEF12,ARPC2,ARPC3,PIP4K2A,RHOF	0.030
			Actin Cytoskeleton Signaling	ARRGFEF12,ARPC2,ARPC3,DIAPH1,MPRIIP	0.038
			Signaling by Rho Family GTPases	ARRGFEF12,ARPC2,ARPC3,PIP4K2A,RHOF	0.046
Females		Actin Nucleation by ARP-WASP Complex	ARPC2,ARPC3,RHOF	0.068	
		Integrin Signaling	ARPC2,ARPC3,MPRIIP,RHOF	0.074	
		Reelin Signaling in Neurons	ARRGFEF12,ARPC2,ARPC3	0.100	
		Rac Signaling	ARPC2,ARPC3,PIP4K2A	0.112	
		INOS Signaling	CHUK,IFNGR1	0.118	

Table 3: Comparison of Regression Model Estimates. Models were fit on the full COPD Data set ($N = 216$).

Variable	Estimate	95% CI	P-value	R^2	Adjusted R^2
ERF				0.140	0.119
Intercept	0.017	-0.150, 0.184	0.845		
Age	0.034	-0.092, 0.160	0.598		
Gender (Female vs Male)	0.006	-0.247, 0.259	0.964		
Race (African American vs White)	-0.345	-0.899, 0.209	0.223		
BMI	0.348	0.219, 0.476	<0.001		
Pack Years	0.018	-0.111, 0.147	0.782		
ERF + Common Protein Score				0.208	0.185
Intercept	0.008	-0.153, 0.169	0.924		
Age	0.057	-0.064, 0.179	0.357		
Gender (Female vs Male)	0.003	-0.240, 0.246	0.982		
Race (African American vs White)	-0.163	-0.702, 0.376	0.555		
BMI	0.350	0.227, 0.473	<0.001		
Pack Years	0.015	-0.108, 0.139	0.807		
Common Protein Score	0.266	0.143, 0.388	<0.001		
ERF + Common Gene Score				0.158	0.134
Intercept	0.017	-0.148, 0.183	0.837		
Age	0.034	-0.091, 0.159	0.598		
Gender (Female vs Male)	0.006	-0.244, 0.257	0.962		
Race (African American vs White)	-0.359	-0.908, 0.190	0.201		
BMI	0.312	0.181, 0.443	<0.001		
Pack Years	0.003	-0.126, 0.131	0.969		
Common Gene Score	0.144	0.014, 0.273	0.031		
ERF + Common Scores				0.229	0.203
Intercept	0.008	-0.150, 0.167	0.917		
Age	0.057	-0.063, 0.178	0.350		
Gender (Female vs Male)	0.003	-0.237, 0.243	0.981		
Race (African American vs White)	-0.175	-0.708, 0.359	0.522		
BMI	0.312	0.186, 0.438	<0.001		
Pack Years	-0.001	-0.124, 0.122	0.985		
Common Protein Score	0.270	0.149, 0.392	<0.001		
Common Gene Score	0.152	0.027, 0.277	0.018		
ERF + Subgroup Protein Score				0.232	0.210
Intercept	0.004	-0.154, 0.162	0.961		
Age	0.059	-0.060, 0.179	0.333		
Gender (Female vs Male)	0.001	-0.238, 0.241	0.991		
Race (African American vs White)	-0.082	-0.616, 0.453	0.765		
BMI	0.336	0.214, 0.458	<0.001		
Pack Years	0.017	-0.105, 0.139	0.786		
Subgroup Protein Score	0.311	0.190, 0.433	<0.001		
ERF + Subgroup Gene Score				0.161	0.137
Intercept	0.017	-0.148, 0.182	0.841		
Age	0.031	-0.093, 0.156	0.624		
Gender (Female vs Male)	0.006	-0.244, 0.256	0.963		
Race (African American vs White)	-0.350	-0.899, 0.198	0.212		
BMI	0.303	0.171, 0.436	<0.001		
Pack Years	0.001	-0.127, 0.129	0.988		
Subgroup Gene Score	0.155	0.024, 0.287	0.021		
ERF + Subgroup Scores				0.257	0.232
Intercept	0.004	-0.152, 0.160	0.960		
Age	0.057	-0.061, 0.175	0.346		
Gender (Female vs Male)	0.001	-0.235, 0.237	0.991		
Race (African American vs White)	-0.082	-0.609, 0.445	0.760		
BMI	0.288	0.163, 0.413	<0.001		
Pack Years	-0.002	-0.123, 0.119	0.979		
Subgroup Protein Score	0.317	0.197, 0.437	<0.001		
Subgroup Gene Score	0.167	0.043, 0.291	0.009		

the data were split into training and testing sets. We divided the data into training (60%) and testing (40%) while keeping the proportions of males and females. Each model was trained on the training data, and we predicted AWT using the testing data. We repeated this process 100 times to reduce variability due to random splitting. We report average R^2 , Adjusted R^2 , and MSEs in Table 4 for the models above plus ERF + Opposite Protein Score, ERF + Opposite Gene Score, and ERF + Opposite Protein and Gene Scores. The average Adjusted R^2 and R^2 from resampling are comparable to the full data.

As expected, the training MSEs were smaller than the testing MSEs. On average, the common scores did not improve test MSEs as much as the subgroup scores. We note the similarity in performance of subgroup, common, and opposite gene score is likely due to the large overlap between the genes selected for each subgroup. When considering Opposite Protein Score, the test MSEs increased indicating worse performance compared to the common and subgroup specific models. Further, the R^2 and Adjusted R^2 were only slightly higher than the ERF model, which shows that the opposite subgroup scores do not contribute much beyond the ERF model. These findings suggest that the proteins and genes we identified to be common and specific to males and females potentially could be explored to further our understanding of sex differences in COPD mechanisms.

6 Conclusion

We have tackled the problem of accounting for subgroup heterogeneity in an integrative analysis framework. Motivated by the COPDGene study and a scientific need to understand sex differences in COPD, we developed appropriate statistical methods that leverage the strengths of multi-view data, account for subgroup heterogeneity, incorporate clinical covariates, and combine the association step with a clinical outcome step to guide the selection of clinically meaningful molecular signatures. Through the use of a hierarchical penalty, we identify omics signatures that are common and subgroup-specific and can predict a clinical outcome. HIP showed comparable to substantially improved prediction and variable selection performance in simulation settings when compared to existing methods.

When we applied HIP to genomic and proteomic data from COPDGene, we identified protein and gene biomarkers and pathways common and specific to males and females. When the proteins and genes were developed into scores, the common and subgroup-specific scores were statistically significant predictors of airway wall thickness (AWT). Further, the scores improved prediction of AWT when added to established COPD risk factors (ERF) compared to ERF alone; the test MSEs were lower, and the amount of variation in AWT explained by the ERF + Subgroup Protein Score model was almost twice the amount of variation in AWT attributable to the ERF model. Notably, when the scores for the subgroups were switched, the amount of variation explained was comparable to the ERF model. These findings suggest the proteins and genes identified to be common and specific to males and females could be explored to further our understanding of sex differences in COPD mechanisms.

HIP has some limitations warranting further research. First, the tuning range for λ_ϵ and λ_g is not determined by the data, so the tuning range may need to be adjusted to attain optimal sparsity. This can be done with an optional parameter in the code. Second, the number of latent components, K , needs to be specified. We provide two methods of selecting this value, but it is impossible to know the correct value of K in applied analyses, and it

Table 4: Average Train and Test MSEs. The data was split 100 times into a test and training set.

Model	Train MSE			Test MSE			R^2	Adjusted R^2
	Overall	Subgroup 1	Subgroup 2	Overall	Subgroup 1	Subgroup 2		
	ERF	0.833	0.887	0.762	0.917	0.970		
ERF + Common Protein Score	0.761	0.802	0.704	0.873	0.905	0.829	0.224	0.186
ERF + Common Gene Score	0.811	0.849	0.761	0.910	0.947	0.860	0.174	0.133
ERF + Common Scores	0.737	0.757	0.710	0.860	0.867	0.852	0.248	0.204
ERF + Subgroup Protein Score	0.738	0.785	0.674	0.847	0.886	0.794	0.247	0.210
ERF + Subgroup Gene Score	0.809	0.847	0.758	0.906	0.941	0.859	0.176	0.135
ERF + Subgroup Scores	0.711	0.728	0.688	0.830	0.831	0.828	0.274	0.232
ERF + Opposite Subgroup Protein Score	0.805	0.826	0.777	0.908	0.930	0.877	0.179	0.139
ERF + Opposite Subgroup Gene Score	0.816	0.853	0.766	0.914	0.952	0.861	0.169	0.128
ERF + Opposite Subgroup Scores	0.783	0.786	0.780	0.895	0.902	0.886	0.201	0.155

may differ by data view. Finally, HIP is limited to cross-sectional data, but future work could extend it to accommodate longitudinal data to determine whether trends in some outcome vary by subgroup. Despite these limitations, HIP advances statistical methods for joint association and prediction of multi-view data, and the encouraging simulation and real data findings motivate further applications.

Funding and Acknowledgements

The project described was supported by Award Numbers 5KL2TR002492-04 from the National Center For Advancing Translational Science, 1R35GM142695-01 from the National Institute Of General Medical Sciences, U01 HL089897 and Award Number U01 HL089856 from the National Heart, Lung, and Blood Institute. COPDGene is also supported by the COPD Foundation through contributions made to an Industry Advisory Board that has included AstraZeneca, Bayer Pharmaceuticals, Boehringer-Ingelheim, Genentech, Glaxo-SmithKline, Novartis, Pfizer, and Sunovion.

Disclaimer: The views expressed in this article are those of the authors and do not reflect the views of the United States Government, the Department of Veterans Affairs, the funders, the sponsors, or any of the authors' affiliated academic institutions.

Data Availability Statement

Access to the clinical and genomic data can be requested through dbGaP (IDs: phs000951.v4.p4 and phs000179.v6.p2). The proteomic data can be requested from the COPDGene Study Group (<http://www.copdgene.org/>)

Supporting Information

Web Tables and Figures referenced in Sections 3.3, 4.1, 4.5, 4.6, 5.2, and 5.3 are available in supporting material. The Python source code for implementing the methods and generating simulated data along with README files are available on GitHub at <https://github.com/lasandrall/HIP>.

References

- Barnes, P. J. (2016), 'Sex differences in chronic obstructive pulmonary disease mechanisms'.
- Beck, A. and Teboulle, M. (2009), 'A fast iterative shrinkage-thresholding algorithm for linear inverse problems', *SIAM J. Img. Sci.* **2**(1), 183?202.
URL: <https://doi.org/10.1137/080716542>
- Bergstra, J. and Bengio, Y. (2012), 'Random search for hyper-parameter optimization', *Journal of Machine Learning Research* **13**(Feb), 281–305.
- Chekouo, T. and Safo, S. E. (2020), 'Bayesian integrative analysis and prediction with application to atherosclerosis cardiovascular disease'.

- Chen, J., Bardes, E. E., Aronow, B. J. and Jegga, A. G. (2009), ‘ToppGene Suite for gene list enrichment analysis and candidate gene prioritization’, *Nucleic Acids Research* **37**(suppl2), W305–W311.
URL: <https://doi.org/10.1093/nar/gkp427>
- Cukic, V., Lovre, V., Dragisic, D. and Ustamujic, A. (2012), ‘Asthma and chronic obstructive pulmonary disease (copd) – differences and similarities’, *Mater Sociomed* **24**(2), 100–105. PMID: 23678316.
- Dondelinger, F., Mukherjee, S. and Initiative, T. A. D. N. (2018), ‘The joint lasso: high-dimensional regression for group structured data’, *Biostatistics* **21**(2), 219–235. eprint: <https://academic.oup.com/biostatistics/article-pdf/21/2/219/32914593/kxy035.pdf>.
URL: <https://doi.org/10.1093/biostatistics/kxy035>
- Dondelinger, F. and Wilkinson, O. (2018), *fuser: Fused Lasso for High-Dimensional Regression over Groups*. R package version 1.0.1.
URL: <https://CRAN.R-project.org/package=fuser>
- Duchi, J., Hazan, E. and Singer, Y. (2011), ‘Adaptive subgradient methods for online learning and stochastic optimization’, *Journal of Machine Learning Research* **12**(61), 2121–2159.
URL: <http://jmlr.org/papers/v12/duchi11a.html>
- Friedman, J., Hastie, T. and Tibshirani, R. (2010), ‘Regularization paths for generalized linear models via coordinate descent’, *Journal of Statistical Software* **33**(1), 1–22.
URL: <http://www.jstatsoft.org/v33/i01/>
- Gan, W. Q., Man, S. P., Postma, D. S., Camp, P. and Sin, D. D. (2006), ‘Female smokers beyond the perimenopausal period are at increased risk of chronic obstructive pulmonary disease: a systematic review and meta-analysis’, *Respiratory research* **7**(1), 1–9.
- GOLD (2020), ‘GOLD 2020 Report Accessed May 20, 2020’, <https://goldcopd.org/wp-content/uploads/2019/11/GOLD-2020-REPORT-ver1.1wms.pdf>.
- Guarascio, A. J., Ray, S. M., Finch, C. K. and Self, T. H. (2013), ‘The clinical and economic burden of chronic obstructive pulmonary disease in the usa’, *ClinicoEconomics and outcomes research: CEOR* **5**, 235.
- Kim, Y.-I., Schroeder, J., Lynch, D., Newell, J., Make, B., Friedlander, A., Estépar, R. S. J., Hanania, N. A., Washko, G., Murphy, J. R. et al. (2011), ‘Gender differences of airway dimensions in anatomically matched sites on ct in smokers’, *COPD: Journal of Chronic Obstructive Pulmonary Disease* **8**(4), 285–292.
- Kramer, A., Green, J., Jr., J. P. and Tugendreich, S. (2014), ‘Causal analysis approaches in ingenuity pathway analysis’, *Bioinformatics* **30**(4), 523–530.
URL: <https://doi.org/10.1093/bioinformatics/btt703>
- Li, Q., Wang, S., Huang, C.-C., Yu, M. and Shao, J. (2014), ‘Meta-analysis based variable selection for gene expression data’, *Biometrics* **70**(4), 872–880.

- Liu, J., Ji, S. and Ye, J. (2009), Multi-task feature learning via efficient l2, 1-norm minimization, in ‘Proceedings of the Twenty-Fifth Conference on Uncertainty in Artificial Intelligence’, UAI ’09, AUAI Press, Arlington, Virginia, USA, p. 339–348.
- Luo, C. and Chen, K. (2017), *CVR: Canonical Variate Regression*. R package version 0.1.1.
URL: <https://CRAN.R-project.org/package=CVR>
- Luo, C., Liu, J., Dey, D. K. and Chen, K. (2016), ‘Canonical variate regression’, *Biostatistics* **17**(3), 468–483.
- Paszke, A., Gross, S., Massa, F., Lerer, A., Bradbury, J., Chanan, G., Killeen, T., Lin, Z., Gimelshein, N., Antiga, L., Desmaison, A., Kopf, A., Yang, E., DeVito, Z., Raison, M., Tejani, A., Chilamkurthy, S., Steiner, B., Fang, L., Bai, J. and Chintala, S. (2019), Pytorch: An imperative style, high-performance deep learning library, in H. Wallach, H. Larochelle, A. Beygelzimer, F. d’Alché-Buc, E. Fox and R. Garnett, eds, ‘Advances in Neural Information Processing Systems 32’, Curran Associates, Inc., pp. 8024–8035.
URL: <http://papers.neurips.cc/paper/9015-pytorch-an-imperative-style-high-performance-deep-learning-library.pdf>
- Prescott, E., Bjerg, A., Andersen, P., Lange, P. and Vestbo, J. (1997), ‘Gender difference in smoking effects on lung function and risk of hospitalization for copd: results from a danish longitudinal population study’, *European Respiratory Journal* **10**(4), 822–827.
- Qin, J., Yang, T., Zeng, N., Wan, C., Gao, L., Li, X., Chen, L., Shen, Y. and Wen, F. (2019), ‘Differential coexpression networks in bronchiolitis and emphysema phenotypes reveal heterogeneous mechanisms of chronic obstructive pulmonary disease’, *Journal of Cellular and Molecular Medicine* **23**(10), 6989–6999.
URL: <https://onlinelibrary.wiley.com/doi/abs/10.1111/jcmm.14585>
- Regan, E. A., Hokanson, J. E., Murphy, J. R., Make, B., Lynch, D. A., Beaty, T. H., Curran-Everett, D., Silverman, E. K. and Crapo, J. D. (2011), ‘Genetic epidemiology of copd (copdgene) study design’, *COPD: Journal of Chronic Obstructive Pulmonary Disease* **7**(1), 32–43.
- Ren, Y., Zhang, Y., Fan, L., Jiao, Q., Wang, Y. and Wang, Q. (2019), ‘The cullin4a is up-regulated in chronic obstructive pulmonary disease patient and contributes to epithelial-mesenchymal transition in small airway epithelium’, *Respiratory Research* **20**(84).
- Richens, T. R., Linderman, D. J., Horstmann, S. A., Lambert, C., Xiao, Y.-Q., Keith, R. L., Boé, D. M., Morimoto, K., Bowler, R. P., Day, B. J., Janssen, W. J., Henson, P. M. and Vandivier, R. W. (2009), ‘Cigarette smoke impairs clearance of apoptotic cells through oxidant-dependent activation of rhoa’, *American Journal of Respiratory and Critical Care Medicine* **179**(11), 1011–1021. PMID: 19264974.
URL: <https://doi.org/10.1164/rccm.200807-1148OC>
- Ruder, S. (2016), ‘An overview of gradient descent optimization algorithms’, *CoRR* **abs/1609.04747**.
URL: <http://arxiv.org/abs/1609.04747>

- Safo, S. E., Min, E. J. and Haine, L. (2021), ‘Sparse linear discriminant analysis for multi-view structured data’, *Biometrics* **n/a**(n/a).
URL: <https://onlinelibrary.wiley.com/doi/abs/10.1111/biom.13458>
- Silverman, E. K. (2018), ‘Applying functional genomics to chronic obstructive pulmonary disease’, *Annals of the American Thoracic Society* **15**(Supplement 4), S239–S242.
- Tibshirani, R. (1994), ‘Regression shrinkage and selection via the lasso’, *JOURNAL OF THE ROYAL STATISTICAL SOCIETY, SERIES B* **58**, 267–288.
- Wells, J. M., Parker, M. M., Oster, R. A., Bowler, R. P., Dransfield, M. T., Bhatt, S. P., Cho, M. H., Kim, V., Curtis, J. L., Martinez, F. J., III, R. P., O’Neal, W., Labaki, W. W., Kaner, R. J., Barjaktarevic, I., Han, M. K., Silverman, E. K., Crapo, J. D., Barr, R. G., Woodruff, P., Castaldi, P. J. and Gaggar, A. (2018), ‘Elevated circulating mmp-9 is linked to increased copd exacerbation risk in spiromics and copdgene’, *JCI Insight* **3**(22).
URL: <https://insight.jci.org/articles/view/123614>
- Wheaton, A. G., Cunningham, T. J., Ford, E. S. and Croft, J. B. (2015), ‘Employment and activity limitations among adults with chronic obstructive pulmonary disease?united states, 2013’, *MMWR. Morbidity and mortality weekly report* **64**(11), 289.
- Zou, H. and Hastie, T. (2005), ‘Regularization and variable selection via the elastic net’, *Journal of the Royal Statistical Society, Series B* **67**, 301–320.

Supporting Information for “Accounting for data heterogeneity in integrative analysis and prediction methods: An application to Chronic Obstructive Pulmonary Disease” by J. Butts, C. Wendt, R. Bowler, C.P. Hersh, Q. Long, L. Eberly, and S. E. Safo

November 16, 2021

1 Methods

1.1 λ and K Selection

The optimization problem in equation 2 in the main manuscript depends on tuning parameters $\lambda = (\lambda_G, \lambda_\xi)$. Ideally, one would search over the entire grid space, but this is computationally expensive. Instead, we randomly select grid values from the hyperparameter space to search over. In particular, we create a grid with a steps between $(0, \lambda_{max}]$ for both λ_G and λ_ξ , and we randomly select 15% of the a^2 combinations to search over. However, we provide the option to search over the entire grid. In our simulations, we set $\lambda_{max} = 1$. In order to select a set of λ values, we calculate the Bayesian Information Criterion (BIC) for a given λ : $BIC = -2 \left(\sum_{s=1}^S F(\mathbf{Y}^s, \mathbf{Z}^s, \Theta) + \sum_{d=1}^D \sum_{s=1}^S \|\mathbf{X}^{d,s} - \mathbf{Z}^s \mathbf{B}^{d,s^T}\|_F^2 \right) + \lambda_B \log(N)$, and we choose the $\lambda = (\lambda_G, \lambda_\xi)$ combination that results in the smallest BIC. Here, λ_B is the sum of the number of non-zero rows across each of the $\mathbf{B}^{d,s}$ matrices.

We propose two automatic ways for selecting the number of components, K . In both approaches, we combine all views and subgroups into an $N \times \{p_1 + \dots + p_D\}$ matrix and use SVD to find the eigenvalues which correspond to the amount of variation explained by corresponding components. We then look at the percent change in eigenvalues and add components until the percent change is less than some threshold as this would correspond to the elbow of a scree plot. For the *simple* approach, we stop at the k where this change is smaller than the threshold and set $K = k$. In the *algorithmic* approach, we find k using the simple approach and run our algorithm for $K = k$ and $K = k + 1$. For each K , we find the best combination of tuning parameters (λ_G and λ_ξ) and select the K resulting in the smallest BIC. In the absence of an ideal approach for selecting K , we recommend the *simple* approach due to its computational advantage. Another option is to manually select K based on a scree plot of the concatenated data. We performed sensitivity analyses to determine how the results of the simulations would change based on K and found the results to be robust though computation time increased with the value of K (Figures 1-2).

1.2 K Selection Results

Web Table 1 reports the proportion of times that the true $K = 2$ was selected in simulations, and the proportion of times that these were over- or under-selected for three pre-specified thresholds. All results are based on 20 simulated data sets. The data was simulated with $K = 2$. We observe that both approaches seem to correctly identify the true number of latent components most of the times in the simulation settings under consideration especially when the threshold is set to 0.1, but the simple approach seemed to be slightly better. The 0.05 threshold tended to overestimate the value of K . For the *simple* approach, the threshold of 0.10 seemed to perform the best of the given thresholds. The 0.05 threshold tended to overestimate K , and the 0.15 threshold tended to underestimate K . The *simple* approach performed as well as or better than than the *algorithmic* approach except for in the Partial P3 scenario with a threshold of 0.15.

For the K selection simulations, we looked at how often the correct K was selected, how often K was underestimated, and how often K was overestimated. All results are based on 20 simulated data sets. The data was simulated with $K = 2$. For the *algorithmic* approach, the threshold of 0.10 seemed to select K correctly the most frequently, although the 0.15 threshold was similar. The 0.05 threshold tended to overestimate the value of K . For the *simple* approach, the threshold of 0.10 seemed to perform the best of the given thresholds. The 0.05 threshold tended to overestimate K , and the 0.15 threshold tended to underestimate K . The *simple* approach performed as well as or better than than the algorithmic approach except for in the Partial P3 scenario with a threshold of 0.15. For this reason and the significant computational advantage of this approach, we would recommend the simple approach with a threshold value of 0.10 if the user would like to use an automatic approach.

In the simulated data sets, scree plots suggested using $K = 4$ in the Full Overlap scenarios and $K = 5$ in the Partial Overlap scenarios. We ran the algorithm with these values for K and found the Full Overlap scenario was robust to either choice of K (2 or 4) (Web Figure 1). The Partial Overlap scenario was slightly less robust to the choice of K with the true value performing better (Web Figure 2). The time to run the algorithm also increased with the value of K . For both computational and simplicity reasons, we recommend to choose a smaller value of K when possible. In the absence of an ideal approach for selecting K , we recommend users to implement either approach, but we prefer the *simple* approach due to its computational advantage.

2 More Simulation Results

Web Figure 3 depicts the Full and Partial Overlap Scenarios used in the simulations.

We first report results for Partial Overlap for the Continuous Setting. The results are similar to the Full Overlap, Continuous Setting. Again, the grid and random searches for the HIP provide similar results (Web Figure 4). There is a more distinct advantage for HIP as CVR performs worse than in the Full Overlap scenario with a lower F1 and higher FPR. The other methods perform similarly to CVR in terms of F1. The Joint Lasso has the highest FPR meaning it is selecting a lot of variables that are not important. The Elastic Net and Lasso methods have a lower TPR meaning they are missing a lot of important variables. In terms of test MSE, HIP appears to perform better than existing methods particularly in the P3 setting.

Table 1: Results for K Selection Approaches

We performed an SVD decomposition to calculate the eigenvalues of the concatenated \mathbf{X} matrix. We look at the percent change in variation from one component to the next adding components until the percent change is less than the given threshold. In the *algorithmic* approach, we consider the number of components selected, k , in addition to $k + 1$ as candidate values for K and select based on BIC. In the *simple* approach, we look at the change in percent variation until it drops below the given threshold. Results are based on 20 simulated data sets.

Setting	Algorithmic Approach			Simple Approach		
	Correct	Over	Under	Correct	Over	Under
Threshold = 0.05						
Full P1	0.30	0.70	0.00	0.30	0.70	0.00
Full P3	0.65	0.35	0.00	0.65	0.35	0.00
Partial P1	0.35	0.65	0.00	0.40	0.60	0.00
Partial P3	0.55	0.40	0.05	0.70	0.25	0.05
Threshold = 0.10						
Full P1	0.75	0.25	0.00	0.75	0.25	0.00
Full P3	1.00	0.00	0.00	1.00	0.00	0.00
Partial P1	0.65	0.30	0.05	0.80	0.15	0.05
Partial P3	0.55	0.20	0.25	0.55	0.00	0.45
Threshold = 0.15						
Full P1	0.85	0.15	0.00	0.85	0.15	0.00
Full P3	0.85	0.00	0.15	0.85	0.00	0.15
Partial P1	0.65	0.20	0.15	0.70	0.00	0.30
Partial P3	0.45	0.00	0.55	0.00	0.00	1.00

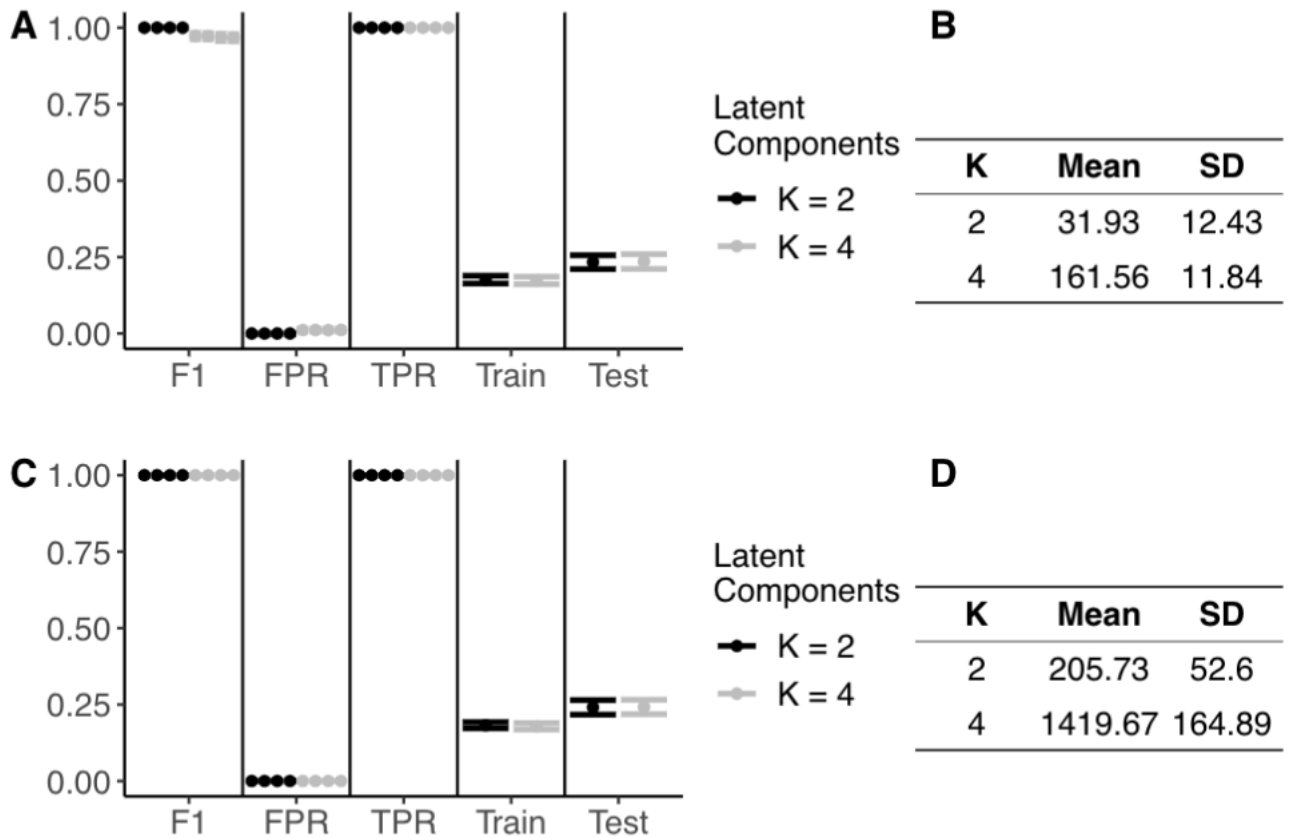


Figure 1: Sensitivity of K for Full Overlap Scenario

(A) Performance of K values in P1 Scenario. (B) Time (in seconds) to run the algorithm in P1 Scenario. (C) Performance of K values in P3 Scenario. (D) Time (in seconds) to run the algorithm in P3 Scenario. All results are summarized over 20 simulated data sets.

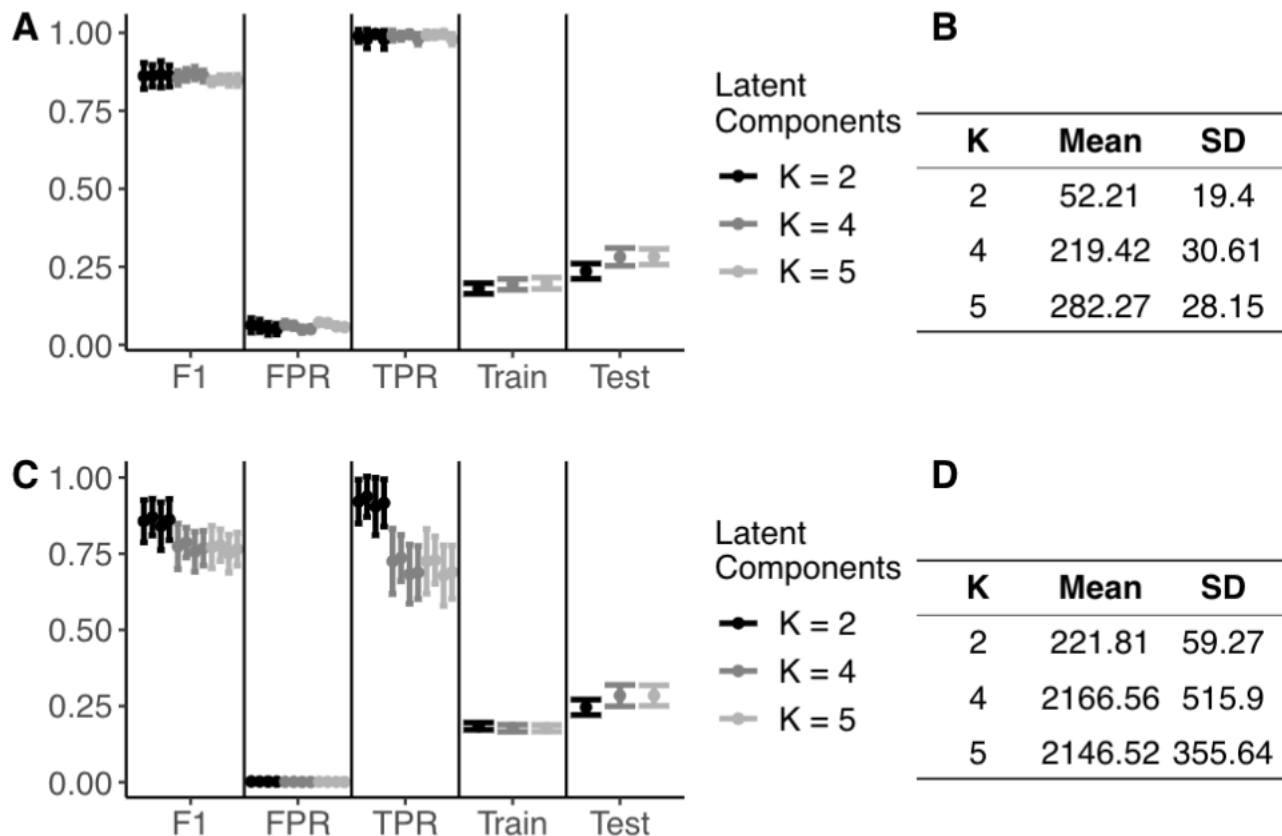


Figure 2: Sensitivity of K for Partial Overlap Scenario

(A) Performance of K values in P1 Scenario. (B) Time (in seconds) to run the algorithm in P1 Scenario. (C) Performance of K values in P3 Scenario. (D) Time (in seconds) to run the algorithm in P3 Scenario. All results are summarized over 20 simulated data sets.

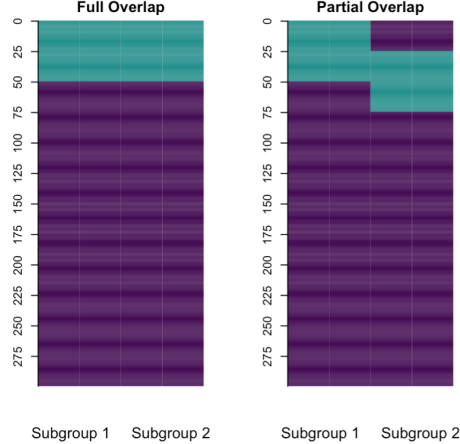


Figure 3: Two Simulation Scenarios. Structure of $\mathbf{B}^{d,s}$, $d, s = 1, 2$ matrices for P1 setting. Teal corresponds to non-zero entries (signals) in the matrix, and purple corresponds to zero entries (noise) in the matrix. In the Full Overlap scenarios, the variables that are important completely overlap in the two subgroups. In the Partial Overlap Scenario, 25 signal variables overlap in the two subgroups.

In terms of computation time, the Lasso and Elastic Net methods are the fastest across all parameter settings followed by HIP (Random). In the P1 setting, HIP (Grid), CVR, and Joint Lasso perform similarly. However, in the P2 setting, we begin to see an advantage for HIP especially for the random search. In the P3 scenario, the Joint Lasso takes a very long time to run.

In the binary simulations, we could not compare with Joint Lasso as it does not accept binary outcomes; otherwise we used the same comparisons. For the binary outcome in the Full Overlap scenario, HIP had higher F1s, lower FPRs, and higher TPRs. Feature selection results for CVR were more variable. The Elastic Net and Lasso both performed similarly to each other; they both had a low TPR meaning that they did not select many of the variables that were important. In terms of test classification accuracy, all methods performed similarly on average, but our method had less variability suggesting more consistent performance.

For the binary outcome in the Partial Overlap Scenario, CVR is the most comparable method but still does not perform as well or as consistently as HIP. The Elastic Net and Lasso methods perform worse as the parameter dimensions increase and tend to miss a lot of important variables. There is some advantage in classification accuracy for HIP as the mean tends to be slightly higher and the variability lower than the existing methods.

In terms of computation time, the Elastic Net and Lasso methods were again the fastest followed by HIP (Random) for both Full and Partial Overlap Scenarios. The improvement in performance is worth the slightly longer computation times. CVR quickly becomes infeasible as the parameter dimensions increase.

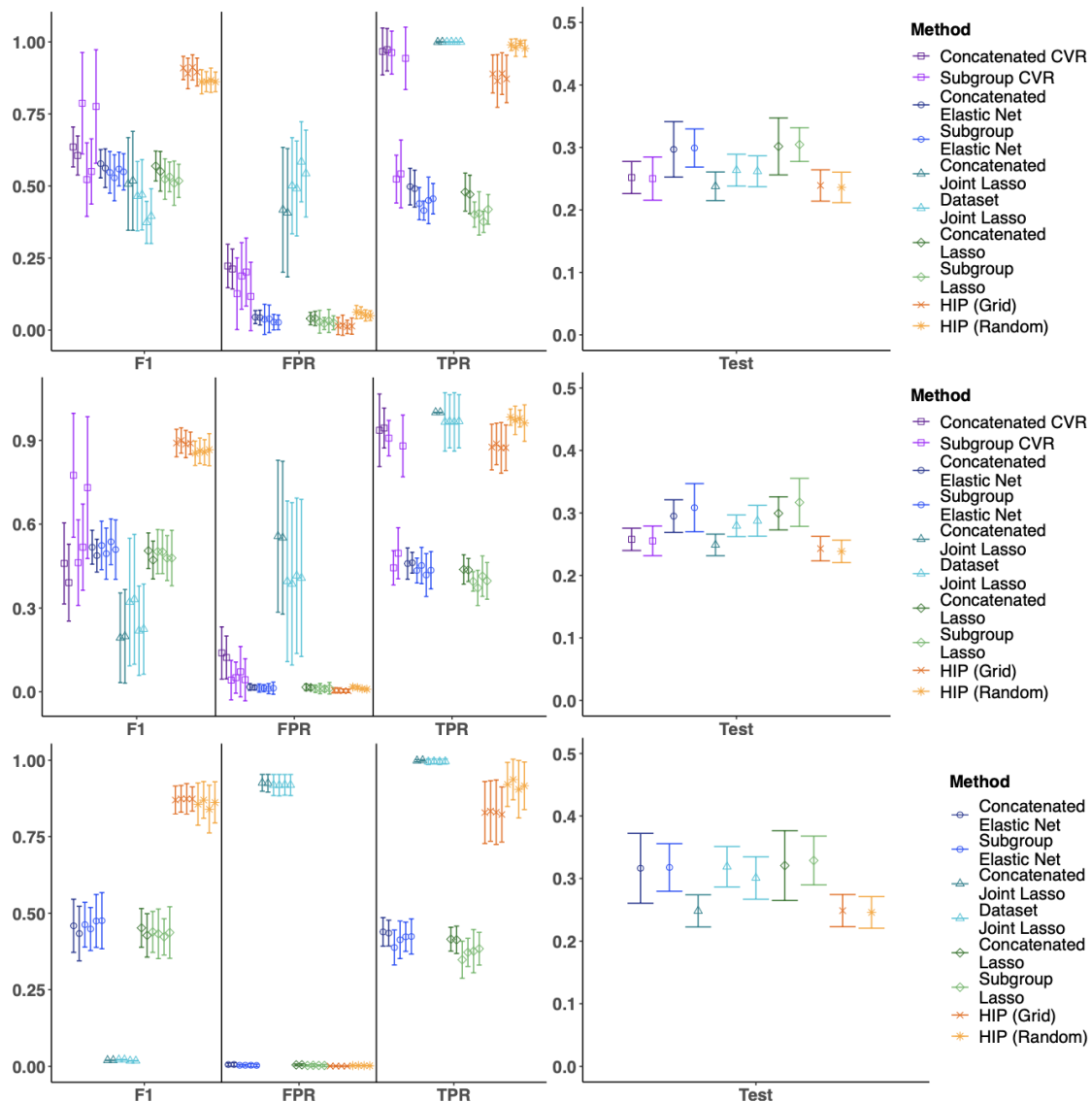


Figure 4: Results for Continuous Outcome, Partial Overlap Scenario

The first row corresponds to P1 ($p_1 = 300$, $p_2 = 350$), the second to P2 ($p_1 = 1000$, $p_2 = 1500$), and the third to P3 ($p_1 = 5000$, $p_2 = 6000$). For all settings, $n_1 = 250$ and $n_2 = 260$. The right column is test mean squared error (MSE), so a lower value indicates better prediction. All results are based on 20 iterations. Results for CVR are not reported for the P3 setting because the computational requirements render the model infeasible.

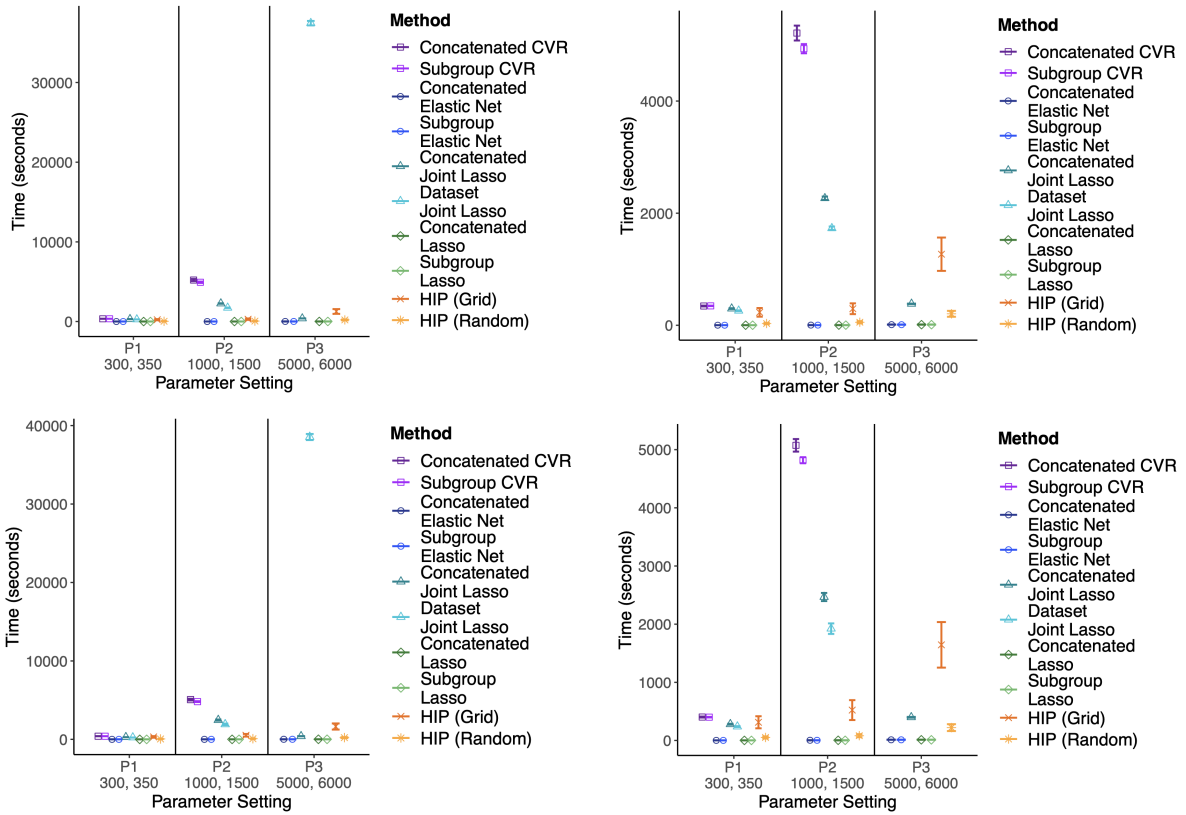


Figure 5: Computation Time for Continuous Outcome. Full Overlap Scenario (Top Panel) and Partial Overlap Scenario (Bottom Panel). (Left) shows computation times for all reported methods. (Right) shows computation times with P3 Dataset Joint Lasso removed to better see the trends. In all figures, CVR is not reported for the P3 setting because the computational requirements render the method infeasible.

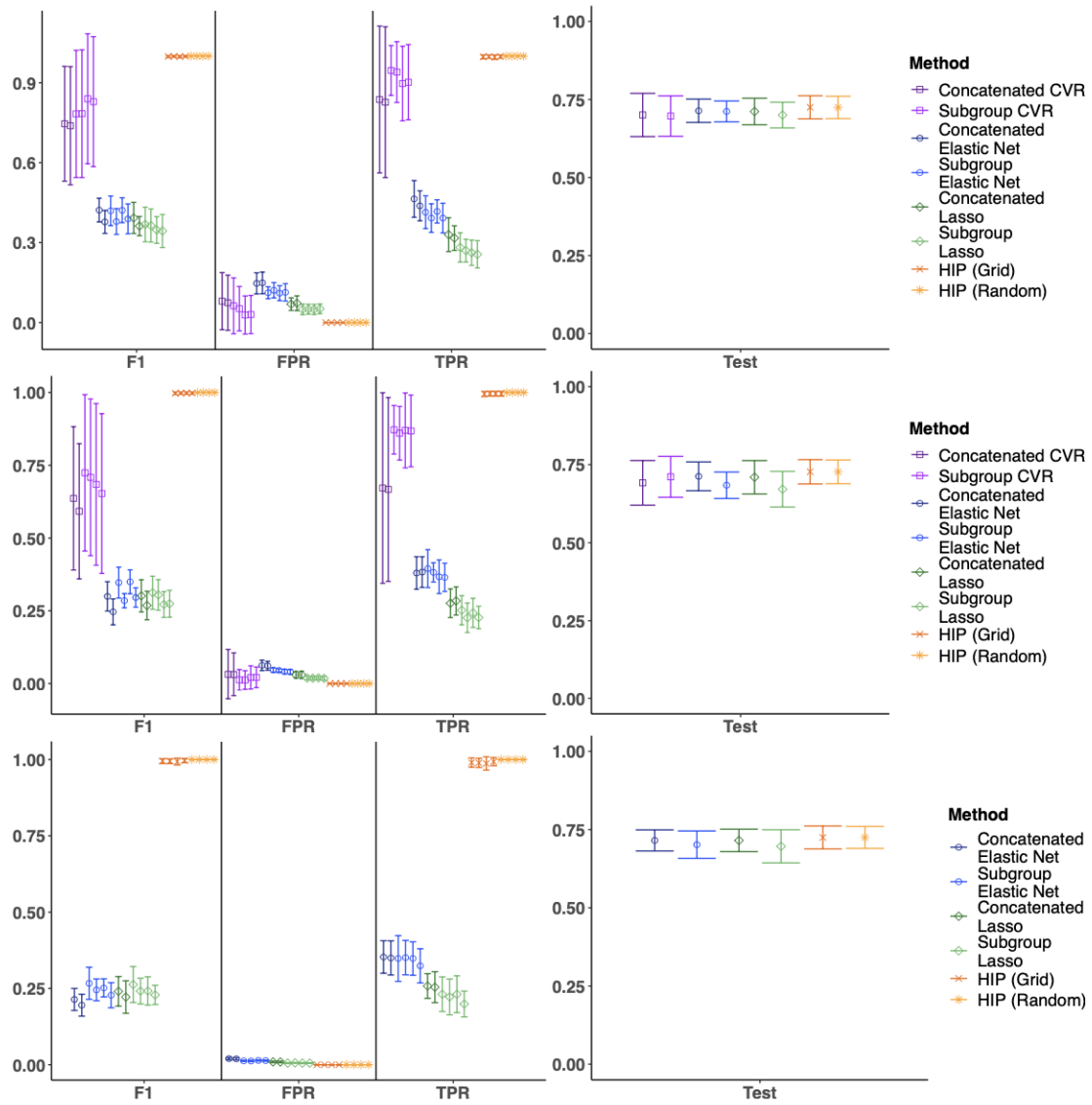


Figure 6: Results for Binary Outcome, Full Overlap Scenario
 The first row corresponds to P1 ($p_1 = 300, p_2 = 350$), the second to P2 ($p_1 = 1000, p_2 = 1500$), and the third to P3 ($p_1 = 5000, p_2 = 6000$). For all settings, $n_1 = 250$ and $n_2 = 260$. The right column is test classification accuracy, so a higher value indicates better prediction. All results are based on 20 iterations. Results for CVR are not reported for the P3 setting because the computational requirements render the model infeasible.

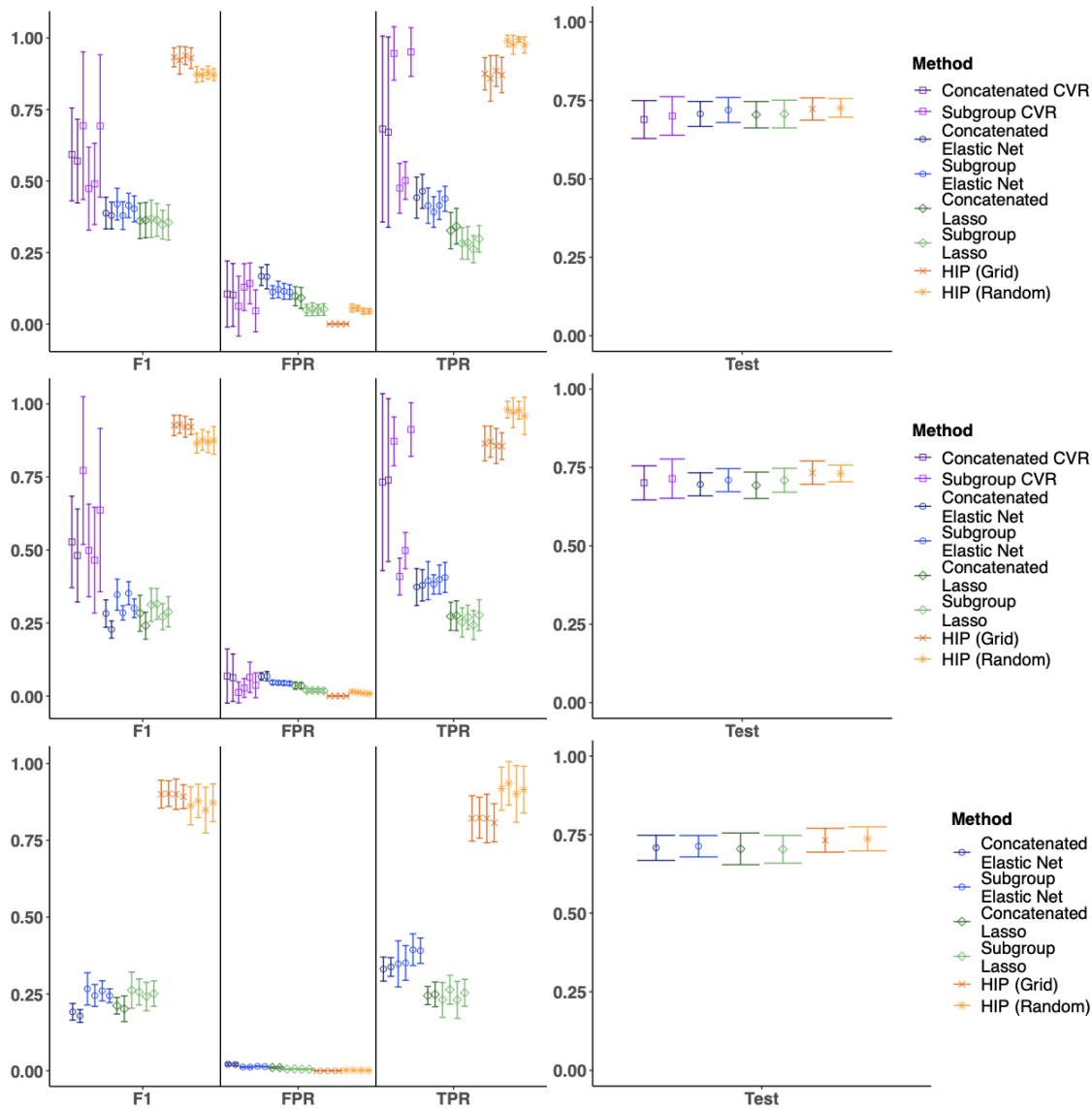


Figure 7: Results for Binary Outcome, Partial Overlap Scenario

The first row corresponds to P1 ($p_1 = 300, p_2 = 350$), the second to P2 ($p_1 = 1000, p_2 = 1500$), and the third to P3 ($p_1 = 5000, p_2 = 6000$). For all settings, $n_1 = 250$ and $n_2 = 260$. The right column is test classification accuracy, so a higher value indicates better prediction. All results are based on 20 iterations. Results for CVR are not reported for the P3 setting because the computational requirements render the model infeasible.

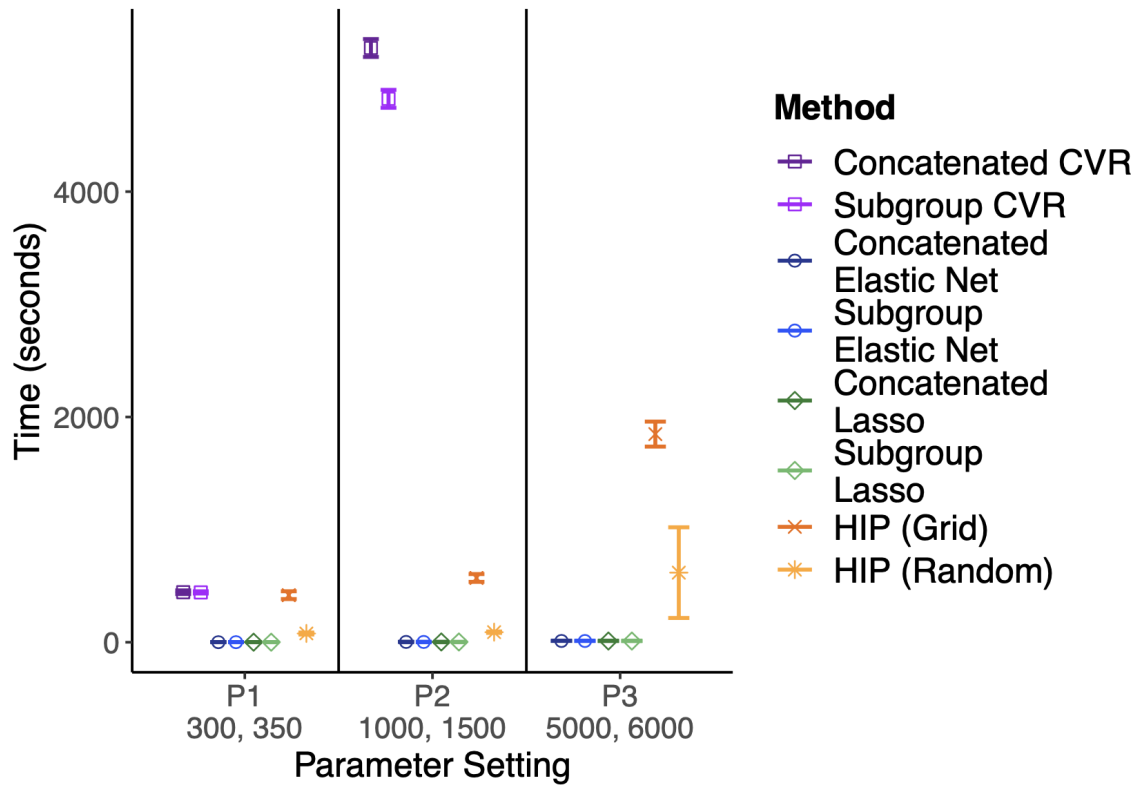


Figure 8: Computation Time for Binary Outcome, Full Overlap Scenario

The Lasso and Elastic Net are the fastest methods across all parameter settings followed by the proposed method with random search. In the P1 setting, CVR and HIP (Grid) perform similarly, but in the P2 setting, the time required by CVR increases dramatically. Results for CVR are not reported for the P3 setting because the computational requirements render the model infeasible.

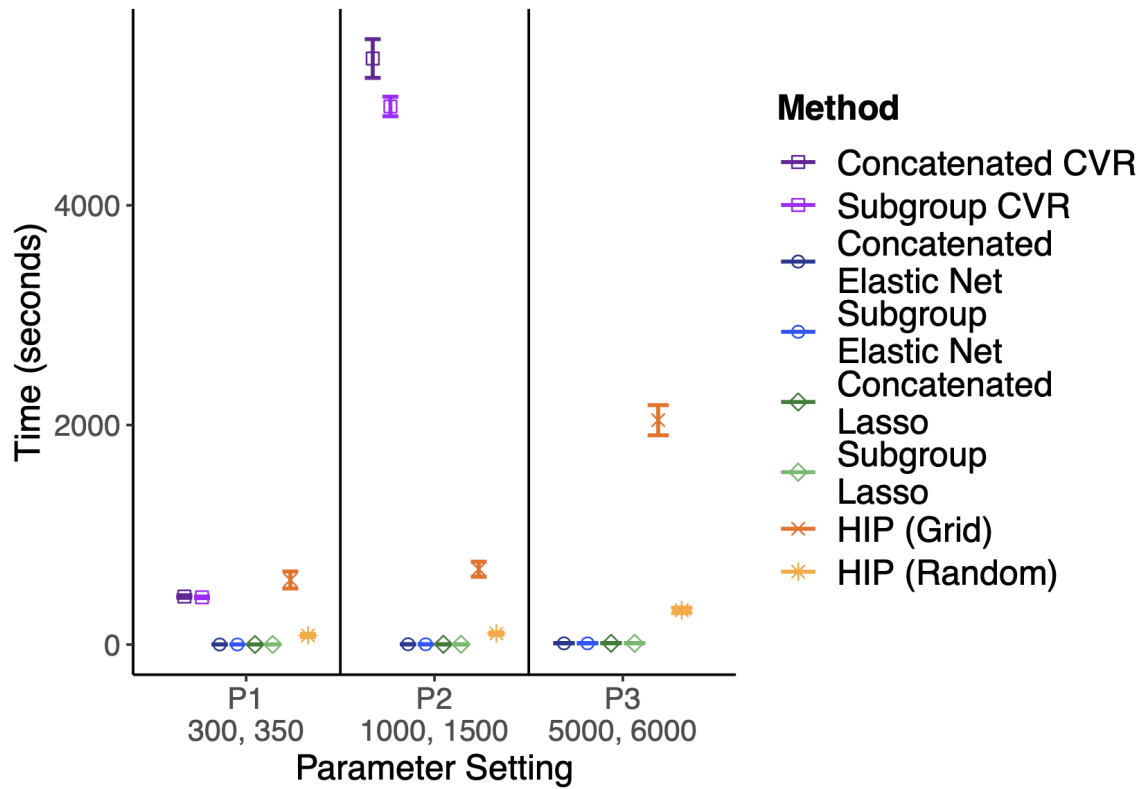


Figure 9: Computation Time for Binary Outcome, Partial Overlap Scenario
 The Lasso and Elastic Net are the fastest methods across all parameter settings followed by the proposed method with random search. In the P1 setting, CVR and HIP (Grid) perform similarly, but in the P2 setting, the time required by CVR increases dramatically. Results for CVR are not reported for the P3 setting because the computational requirements render the model infeasible.

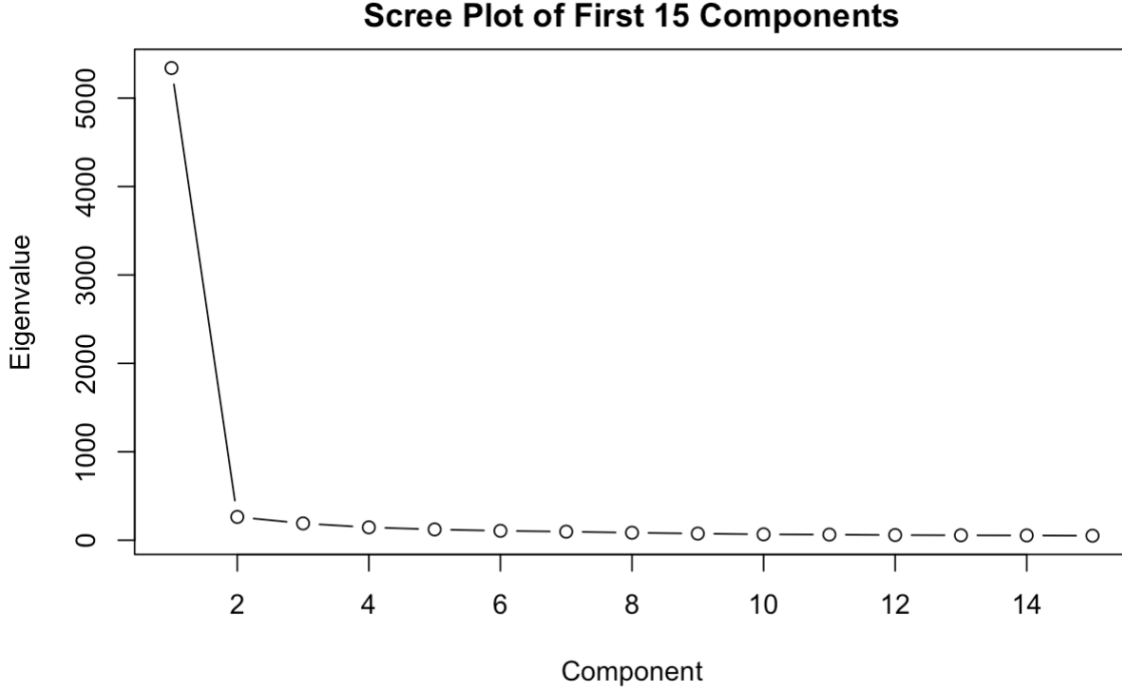


Figure 10: Scree plot of concatenated data matrix for real data analysis

3 Real Data Analysis

Here we report some additional findings from the data application using the COPDGene data. Web Figure 10 shows the scree plot for the unstandardized concatenated data which suggests a $K = 4$. Web Figure 11 shows the Test MSEs from each method on the fifty bootstrap data sets. Web Figure 12 shows the overlap of variables selected by each method. None of the genes that were selected as important to males and females by HIP (Random) overlapped with Elastic Net. There were 2 overlapping genes for males and 0 for females with CVR. There were 10 overlaps for males and 1 overlap for females with Joint Lasso. For the proteins identified as important to males by HIP, 10 overlapped with CVR, 11 with Joint Lasso, and 1 with Elastic net. For the proteins identified for females, 4 overlapped with Joint Lasso, 6 overlapped with CVR, and 1 overlapped with Elastic Net.

Web Table 2 lists the proteins selected by HIP (Random) for males and females in addition to the average weights calculated from the $\mathbf{B}^{d,s}$ matrices. The genes selected by HIP (Random) are listed in Web Table 3 for males and Web Table 4 for females. Web Table 5 lists the gene ontology biological processes that were enriched in our protein list for males and females. Web Table 6 shows the number of variables selected for each method and how many overlapped between males and females. HIP (Random) selected 34 and 30 proteins as important to males and females respectively, with 28 of these proteins common between the two subgroups. Sixty-six genes were selected as important to males and 60 genes were selected as important to females, with 6 of these genes common between the two subgroups. Web Table 7 shows the number of variables selected by HIP (Grid) and HIP (Random) and how many of the selected variables overlapped.

Table 2: List of Proteins Selected by HIP (Random) in COPD Application. Weights are coefficients from the estimated $B^{d,s}$ matrices. Higher values suggest that the variable likely contribute more to association and prediction.

Subgroup	ID	Name	Symbol	Weight
Males	2026	Gamma-enolase	ENO2	0.094
	23767	Leucine-rich repeat transmembrane protein FLRT3	FLRT3	0.365
	8349	Histone H2B type 2-E	HIST2H2BE	0.087
	3146	High mobility group protein B1	HMGB1	0.062
	4318	Matrix metalloproteinase-9	MMP9	0.613
	4916	NT-3 growth factor receptor	NTRK3	0.119
	3489	Insulin-like growth factor-binding protein 6	IGFBP6	0.064
	5623	Persephin	PSPN	0.066
	6469	Sonic hedgehog protein	SHH	0.151
	3624	Inhibin beta A chain	INHBA	0.070
	56729	Resistin	RETN	0.097
	7133	Tumor necrosis factor receptor superfamily member 1B	TNFRSF1B	0.204
	3423	Iduronate 2-sulfatase	IDS	0.157
	6422	Secreted frizzled-related protein 1	SFRP1	0.152
	7045	Transforming growth factor-beta-induced protein ig-h3	TGFB1	0.069
	633	Biglycan	BGN	0.165
	135228	CD109 antigen	CD109	0.323
	4063	T-lymphocyte surface antigen Ly-9	LY9	0.404
	23705	Cell adhesion molecule 1	CADM1	0.479
	2799	N-acetylglucosamine-6-sulfatase	GNS	0.168
	671	Bactericidal permeability-increasing protein	BPI	0.113
	79077	dCTP pyrophosphatase 1	DCCTPP1	0.181
	91653	Brother of CDO	BOC	0.237
	6441	Pulmonary surfactant-associated protein D	SFTPD	0.309
	7169	Tropomyosin beta chain	TPM2	0.085
	50937	Cell adhesion molecule-related/down-regulated by oncogenes	CDON	0.103
	26050	SLIT and NTRK-like protein 5	SLITRK5	0.177
	2022	Endoglin	ENG	0.419
	57556	Semaphorin-6A	SEMA6A	0.294
	7297	Tyrosine Kinase 2	TYK2	0.082
	1991	Elastase, Neutrophil Expressed	ELANE	0.083
	6280	S100 Calcium Binding Protein A9	S100A9	0.163
	6283	S100 Calcium Binding Protein A12	S100A12	0.073
	7327	Ubiquitin Conjugating Enzyme E2 G2	UBE2G2	0.106
	Females	2026	Gamma-enolase	ENO2
23767		Leucine-rich repeat transmembrane protein FLRT3	FLRT3	0.178
3146		High mobility group protein B1	HMGB1	0.033
4318		Matrix metalloproteinase-9	MMP9	0.370
4916		NT-3 growth factor receptor	NTRK3	0.067
3489		Insulin-like growth factor-binding protein 6	IGFBP6	0.106
6469		Sonic hedgehog protein	SHH	0.274
3624		Inhibin beta A chain	INHBA	0.129
7133		Tumor necrosis factor receptor superfamily member 1B	TNFRSF1B	0.277
3423		Iduronate 2-sulfatase	IDS	0.131
6422		Secreted frizzled-related protein 1	SFRP1	0.178
7045		Transforming growth factor-beta-induced protein ig-h3	TGFB1	0.261
633		Biglycan	BGN	0.192
135228		CD109 antigen	CD109	0.196
4063		T-lymphocyte surface antigen Ly-9	LY9	0.470
23705		Cell adhesion molecule 1	CADM1	0.335
2799		N-acetylglucosamine-6-sulfatase	GNS	0.159
6449		Small glutamine-rich tetratricopeptide repeat-containing protein alpha	SGTA	0.083
671		Bactericidal permeability-increasing protein	BPI	0.083
79077		dCTP pyrophosphatase 1	DCCTPP1	0.132
91653		Brother of CDO	BOC	0.125
6441		Pulmonary surfactant-associated protein D	SFTPD	0.336
7169		Tropomyosin beta chain	TPM2	0.098
50937		Cell adhesion molecule-related/down-regulated by oncogenes	CDON	0.117
26050		SLIT and NTRK-like protein 5	SLITRK5	0.248
2022		Endoglin	ENG	0.407
57556		Semaphorin-6A	SEMA6A	0.225
1991		Elastase, Neutrophil Expressed	ELANE	0.080
6280		S100 Calcium Binding Protein A9	S100A9	0.163
10082		Glypican 6	GPC6	0.108

Table 3: List of Genes Selected by HIP (Random) for Males in COPD Application. Weights are coefficients from the estimated $B^{d,s}$ matrices. Higher values suggest that the variable likely contribute more to association and prediction.

ID	Name	Symbol	Weight
ENSG00000125257	ATP binding cassette subfamily C member 4	ABCC4	0.048
ENSG00000095139	archain 1	ARCN1	0.028
ENSG00000196914	Rho guanine nucleotide exchange factor 12	ARRHGEF12	0.603
ENSG00000175414	ADP ribosylation factor like GTPase 10	ARL10	0.030
ENSG00000163466	actin related protein 2/3 complex subunit 2	ARPC2	0.028
ENSG00000111229	actin related protein 2/3 complex subunit 3	ARPC3	0.030
ENSG00000113732	ATPase H+ transporting V0 subunit e1	ATP6V0E1	0.046
ENSG00000140299	BCL2 interacting protein 2	BNIP2	0.035
ENSG00000143612	chromosome 1 open reading frame 43	C1orf43	0.019
ENSG00000116489	capping actin protein of muscle Z-line subunit alpha 1	CAPZA1	0.042
ENSG00000198898	capping actin protein of muscle Z-line subunit alpha 2	CAPZA2	0.040
ENSG00000268001	CARD8 antisense RNA 1	CARD8-AS1	0.015
ENSG00000177352	coiled-coil domain containing 71	CCDC71	0.032
ENSG00000004897	cell division cycle 27	CDC27	0.328
ENSG00000213341	component of inhibitor of nuclear factor kappa B kinase complex	CHUK	0.056
ENSG00000213719	chloride intracellular channel 1	CLIC1	0.029
ENSG00000122218	COPI coat complex subunit alpha	COPA	0.042
ENSG00000099942	CRK like proto-oncogene, adaptor protein	CRKL	0.052
ENSG00000009307	cold shock domain containing E1	CSDE1	0.054
ENSG00000139842	cullin 4A	CUL4A	1.614
ENSG00000131504	diaphanous related formin 1	DIAPH1	0.043
ENSG00000086232	eukaryotic translation initiation factor 2 alpha kinase 1	EIF2AK1	0.064
ENSG00000159023	erythrocyte membrane protein band 4.1	EPB41	0.138
ENSG00000133193	family with sequence similarity 104 member A	FAM104A	0.199
ENSG00000116199	FAM20B glycosaminoglycan xylosylkinase	FAM20B	0.034
ENSG00000124098	family with sequence similarity 210 member B	FAM210B	0.035
ENSG00000197601	fatty acyl-CoA reductase 1	FAR1	0.074
ENSG00000225733	FGD5 antisense RNA 1	FGD5-AS1	0.020
ENSG00000001084	glutamate-cysteine ligase catalytic subunit	GCLC	0.275
ENSG00000182512	glutaredoxin 5	GLRX5	0.037
ENSG00000126945	heterogeneous nuclear ribonucleoprotein H2	HNRNPH2	0.051
ENSG00000027697	interferon gamma receptor 1	IFNGR1	0.051
ENSG00000143543	jumping translocation breakpoint	JTB	0.019
ENSG00000114166	lysine acetyltransferase 2B	KAT2B	0.054
ENSG00000170759	kinesin family member 5B	KIF5B	0.021
ENSG00000257103	LSM14A mRNA processing body assembly factor	LSM14A	0.049
ENSG00000165406	membrane associated ring-CH-type finger 8	MARCHF8	0.078
ENSG00000112159	midasin AAA ATPase 1	MDN1	0.030
ENSG00000161013	alpha-1,3-mannosyl-glycoprotein 4-beta-N-acetylglucosaminyltransferase B	MGAT4B	0.029
ENSG00000133606	makorin ring finger protein 1	MKRN1	0.038
ENSG00000133030	myosin phosphatase Rho interacting protein	MPRIP	0.032
ENSG00000119950	MAX interactor 1, dimerization protein	MXI1	0.055
ENSG00000025770	non-SMC condensin II complex subunit H2	NCAPH2	0.037
ENSG00000120265	protein-L-isoaspartate (D-aspartate) O-methyltransferase	PCMT1	0.035
ENSG00000150867	phosphatidylinositol-5-phosphate 4-kinase type 2 alpha	PIP4K2A	0.452
ENSG00000163605	protein phosphatase 4 regulatory subunit 2	PPP4R2	0.043
ENSG00000175166	proteasome 26S subunit, non-ATPase 2	PSMD2	0.067
ENSG00000084733	RAB10, member RAS oncogene family	RAB10	0.022
ENSG00000080371	RAB21, member RAS oncogene family	RAB21	0.022
ENSG00000153250	RNA binding motif single stranded interacting protein 1	RBMS1	0.071
ENSG00000139725	ras homolog family member F, filopodia associated	RHOF	0.024
ENSG00000101782	RIO kinase 3	RIOK3	0.087
ENSG00000196154	S100 calcium binding protein A4	S100A4	0.016
ENSG00000112335	sorting nexin 3	SNX3	0.109
ENSG00000163554	spectrin alpha, erythrocytic 1	SPTA1	0.036
ENSG00000148175	stomatin	STOM	0.074
ENSG00000082146	STE20 related adaptor beta	STRADB	0.068
ENSG00000065491	TBC1 domain family member 22B	TBC1D22B	0.036
ENSG00000174695	transmembrane protein 167A	TMEM167A	0.020
ENSG00000116209	transmembrane protein 59	TMEM59	0.069
ENSG00000124333	vesicle associated membrane protein 7	VAMP7	0.015
ENSG00000149823	VPS51 subunit of GARP complex	VPS51	0.066
ENSG00000100568	vesicle transport through interaction with t-SNAREs 1B	VTI1B	0.165
ENSG00000130227	exportin 7	XPO7	0.193
ENSG00000060138	Y-box binding protein 3	YBX3	0.057
ENSG00000170027	tyrosine 3-monooxygenase/tryptophan 5-monooxygenase activation protein gamma	YWHAQ	0.101

Table 4: List of Genes Selected by HIP (Random) for Females in COPD Application. Weights are coefficients from the estimated $B^{d,s}$ matrices. Higher values suggest that the variable likely contribute more to association and prediction.

ID	Name	Symbol	Weight
ENSG00000125257	ATP binding cassette subfamily C member 4	ABCC4	0.035
ENSG00000196914	Rho guanine nucleotide exchange factor 12	ARHGEF12	0.664
ENSG00000175414	ADP ribosylation factor like GTPase 10	ARL10	0.037
ENSG00000163466	actin related protein 2/3 complex subunit 2	ARPC2	0.035
ENSG00000111229	actin related protein 2/3 complex subunit 3	ARPC3	0.030
ENSG00000113732	ATPase H+ transporting V0 subunit e1	ATP6V0E1	0.045
ENSG00000140299	BCL2 interacting protein 2	BNIP2	0.031
ENSG00000143612	chromosome 1 open reading frame 43	C1orf43	0.022
ENSG00000116489	capping actin protein of muscle Z-line subunit alpha 1	CAPZA1	0.045
ENSG00000198898	capping actin protein of muscle Z-line subunit alpha 2	CAPZA2	0.045
ENSG00000268001	CARD8 antisense RNA 1	CARD8-AS1	0.015
ENSG00000177352	coiled-coil domain containing 71	CCDC71	0.027
ENSG00000004897	cell division cycle 27	CDC27	0.283
ENSG00000213341	component of inhibitor of nuclear factor kappa B kinase complex	CHUK	0.060
ENSG00000213719	chloride intracellular channel 1	CLIC1	0.030
ENSG00000122218	COPI coat complex subunit alpha	COPA	0.018
ENSG00000009307	cold shock domain containing E1	CSDE1	0.058
ENSG00000139842	cullin 4A	CUL4A	1.596
ENSG00000131504	diaphanous related formin 1	DIAPH1	0.052
ENSG000000086232	eukaryotic translation initiation factor 2 alpha kinase 1	EIF2AK1	0.066
ENSG00000159023	erythrocyte membrane protein band 4.1	EPB41	0.093
ENSG00000133193	family with sequence similarity 104 member A	FAM104A	0.183
ENSG00000116199	FAM20B glycosaminoglycan xylosylkinase	FAM20B	0.053
ENSG00000197601	fatty acyl-CoA reductase 1	FAR1	0.080
ENSG00000225733	FGD5 antisense RNA 1	FGD5-AS1	0.022
ENSG00000001084	glutamate-cysteine ligase catalytic subunit	GCLC	0.219
ENSG00000126945	heterogeneous nuclear ribonucleoprotein H2	HNRNPH2	0.054
ENSG00000027697	interferon gamma receptor 1	IFNGR1	0.060
ENSG00000143543	jumping translocation breakpoint	JTB	0.022
ENSG00000114166	lysine acetyltransferase 2B	KAT2B	0.041
ENSG00000170759	kinesin family member 5B	KIF5B	0.022
ENSG00000165406	membrane associated ring-CH-type finger 8	MARCHF8	0.047
ENSG00000112159	midasin AAA ATPase 1	MDN1	0.034
ENSG00000161013	alpha-1,3-mannosyl-glycoprotein 4-beta-N-acetylglucosaminyltransferase B	MGAT4B	0.025
ENSG00000133606	makorin ring finger protein 1	MKRN1	0.032
ENSG00000133030	myosin phosphatase Rho interacting protein	MPRI1	0.028
ENSG00000119950	MAX interactor 1, dimerization protein	MXI1	0.036
ENSG00000025770	non-SMC condensin II complex subunit H2	NCAPH2	0.044
ENSG00000120265	protein-L-isoaspartate (D-aspartate) O-methyltransferase	PCMT1	0.036
ENSG00000150867	phosphatidylinositol-5-phosphate 4-kinase type 2 alpha	PIP4K2A	0.428
ENSG00000163605	protein phosphatase 4 regulatory subunit 2	PPP4R2	0.044
ENSG00000175166	proteasome 26S subunit, non-ATPase 2	PSMD2	0.079
ENSG000000084733	RAB10, member RAS oncogene family	RAB10	0.015
ENSG000000080371	RAB21, member RAS oncogene family	RAB21	0.022
ENSG00000153250	RNA binding motif single stranded interacting protein 1	RBMS1	0.052
ENSG00000139725	ras homolog family member F, filopodia associated	RHOF	0.022
ENSG00000101782	RIO kinase 3	RIOK3	0.060
ENSG00000196154	S100 calcium binding protein A4	S100A4	0.018
ENSG00000112335	sorting nexin 3	SNX3	0.114
ENSG00000163554	spectrin alpha, erythrocytic 1	SPTA1	0.044
ENSG00000148175	stomatin	STOM	0.046
ENSG000000082146	STE20 related adaptor beta	STRADB	0.066
ENSG00000174695	transmembrane protein 167A	TMEM167A	0.025
ENSG00000116209	transmembrane protein 59	TMEM59	0.068
ENSG00000124333	vesicle associated membrane protein 7	VAMP7	0.015
ENSG00000149823	VPS51 subunit of GARP complex	VPS51	0.073
ENSG00000100568	vesicle transport through interaction with t-SNAREs 1B	VTI1B	0.169
ENSG00000130227	exportin 7	XPO7	0.204
ENSG000000060138	Y-box binding protein 3	YBX3	0.026
ENSG00000170027	tyrosine 3-monooxygenase/tryptophan 5-monooxygenase activation protein gamma	YWHAG	0.103

Table 5: Top 10 Gene Ontology Biological Processes using ToppGene Suite

View	Subgroup	GO ID	Biological Process	FDR	B&H P-Value	Molecules
Proteins	Males	GO:0006935	chemotaxis	0.000		BOC,SHH,ELANE,S100A9,HMGB1,S100A12,SEMA6A, SFRP1,GFAPP6,ENG,SFTPD,NTRK3
		GO:0042930	taxis	0.000		BOC,SHH,ELANE,S100A9,HMGB1,S100A12,SEMA6A,FLRT3, ENG,SFTPD,NTRK3,PSFN
		GO:0045321	leukocyte activation	0.000		SHH,ELANE,S100A9,HMGB1,S100A12,SFRP1,RETN,CADMI, TNFRSF1B,MMP9,LY9,BP1,INHBA,SFTPD,GNS
	Females	GO:0001775	cell activation	0.000		SHH,ELANE,S100A9,HMGB1,S100A12,SFRP1,RETN,CADMI, TNFRSF1B,MMP9,LY9,BP1,INHBA,SFTPD,GNS
		GO:0051240	positive regulation of multicellular organismal process	0.000		SLITRK5,SHH,ELANE,S100A9,HMGB1,FLRT3,RETN,CADMI, MMP9,LY9,ENG,INHBA,NTRK3,CDON
		GO:0016477	cell migration	0.000		SHH,ELANE,S100A9,HMGB1,S100A12,SEMA6A,SFRP1,FLRT3,RETN,CADMI, MMP9,GFAPP6,ENG,SFTPD,NTRK3
		GO:0043312	neutrophil degranulation	0.000		ELANE,S100A9,HMGB1,S100A12,RETN,TNFRSF1B,MMP9,BP1,GNS
		GO:0007155	cell adhesion	0.000		BOC,SHH,TFGB1,ELANE,S100A9,HMGB1,SEMA6A,SFRP1,FLRT3, CADMI,LY9,ENG,SFTPD,CDON
		GO:0002283	neutrophil activation involved in immune response	0.000		ELANE,S100A9,HMGB1,S100A12,RETN,TNFRSF1B,MMP9,BP1,GNS
		GO:0022010	biological adhesion	0.000		BOC,SHH,TFGB1,ELANE,S100A9,HMGB1,SEMA6A,SFRP1,FLRT3, CADMI,LY9,ENG,SFTPD,CDON
Genes	Males	GO:0007155	cell adhesion	0.000		BOC,SHH,TFGB1,ELANE,S100A9,HMGB1,SEMA6A,SFRP1,FLRT3, CADMI,LY9,GPC6,ENG,SFTPD,CDON
		GO:0022610	biological adhesion	0.000		BOC,SHH,TFGB1,ELANE,S100A9,HMGB1,SEMA6A,SFRP1,FLRT3, CADMI,LY9,GPC6,ENG,SFTPD,CDON
		GO:0051240	positive regulation of multicellular organismal process	0.000		SLITRK5,SHH,ELANE,S100A9,HMGB1,FLRT3,CADMI,TNFRSF1B, MMP9,LY9,ENG,INHBA,NTRK3,CDON
		GO:0006935	chemotaxis	0.000		BOC,SHH,ELANE,S100A9,HMGB1,SEMA6A,FLRT3,ENG,SFTPD,NTRK3
		GO:0042930	taxis	0.000		BOC,SHH,ELANE,S100A9,HMGB1,SEMA6A,FLRT3,ENG,SFTPD,NTRK3
	Females	GO:0045321	leukocyte activation	0.000		SHH,ELANE,S100A9,HMGB1,SFRP1,CADMI,TNFRSF1B,MMP9,LY9,BP1, INHBA,SFTPD,GNS
		GO:0016477	cell migration	0.000		SHH,ELANE,S100A9,HMGB1,SEMA6A,SFRP1,FLRT3,CADMI,MMP9, GFAPP6,ENG,SFTPD,NTRK3
		GO:0001775	cell activation	0.000		SHH,ELANE,S100A9,HMGB1,SFRP1,CADMI,TNFRSF1B,MMP9,LY9, BP1,INHBA,SFTPD,GNS
		GO:0002695	negative regulation of leukocyte activation	0.000		SHH,HMGB1,SFRP1,BP1,INHBA,SFTPD
		GO:0098609	cell-cell adhesion	0.000		BOC,SHH,ELANE,S100A9,HMGB1,FLRT3,CADMI,GPC6,SFTPD,CDON
Genes	Males	GO:1905475	regulation of protein localization to membrane	0.000		TMEM59,VAMP7,KIF5B,YWHAG,CRKL,STOM,VTIIB,ARPC2
		GO:0048193	Golgi vesicle transport	0.000		RAB10,ABCC4,SNX3,COPA,SPTA1,CAPZA1,VAMP7,CAPZA2, TBC1D22B,VPS51,YWHAG,ARCN1,VTIIB
		GO:0006888	endoplasmic reticulum to Golgi vesicle-mediated transport	0.002		COPA,SPTA1,CAPZA1,VAMP7,CAPZA2,ARCN1,VTIIB
		GO:0022604	regulation of cell morphogenesis	0.005		SPTA1,VAMP7,DIAPH1,RAB21,RHOF,EPB41,CRKL,ARPC2
		GO:0051693	actin filament capping	0.005		SPTA1,CAPZA1,CAPZA2,ARPC2
	Females	GO:0016482	cytosolic transport	0.005		SNX3,PIP4K2A,KIF5B,VPS51,RAB21,VTIIB
		GO:1903827	regulation of cellular protein localization	0.005		SNX3,TMEM59,VAMP7,KIF5B,YWHAG,EPB41,CRKL,STOM,VTIIB,ARPC2
		GO:0030835	negative regulation of actin filament depolymerization	0.005		SNX3,TMEM59,VAMP7,DIAPH1,KIF5B,RAB21,YWHAG,EPB41, CRKL,STOM,VTIIB,ARPC2
		GO:0030941	actin filament polymerization	0.006		SPTA1,CAPZA1,CAPZA2,DIAPH1,ARPC3,ARPC2
		GO:0054775	regulation of protein localization to membrane	0.004		TMEM59,VAMP7,KIF5B,YWHAG,STOM,VTIIB,ARPC2
Genes	Males	GO:0048193	Golgi vesicle transport	0.004		RAB10,ABCC4,SNX3,COPA,SPTA1,CAPZA1,VAMP7,CAPZA2, VPS51,YWHAG,VTIIB
		GO:0016482	cytosolic transport	0.004		SNX3,PIP4K2A,KIF5B,VPS51,RAB21,VTIIB
		GO:0051693	actin filament capping	0.004		SPTA1,CAPZA1,CAPZA2,ARPC2
		GO:0030835	negative regulation of actin filament depolymerization	0.004		SPTA1,CAPZA1,CAPZA2,ARPC2
		GO:0006906	vesicle fusion	0.004		RAB10,ABCC4,PIP4K2A,VAMP7,DIAPH1,PSMD2,KIF5B,RAB21, RHOF,STOM,TMEM167A,VTIIB
	Females	GO:0090174	organelle membrane fusion	0.004		RAB10,ABCC4,PIP4K2A,VAMP7,DIAPH1,PSMD2,KIF5B,RAB21, TMEM167A,VTIIB
		GO:0030941	actin filament polymerization	0.004		SPTA1,CAPZA1,CAPZA2,DIAPH1,ARPC3,ARPC2
		GO:0048284	organelle fusion	0.004		RAB10,ABCC4,PIP4K2A,VAMP7,DIAPH1,PSMD2,KIF5B, RAB21,RHOF,STOM,TMEM167A,VTIIB
		GO:0006888	endoplasmic reticulum to Golgi vesicle-mediated transport	0.004		COPA,SPTA1,CAPZA1,VAMP7,CAPZA2,VTIIB

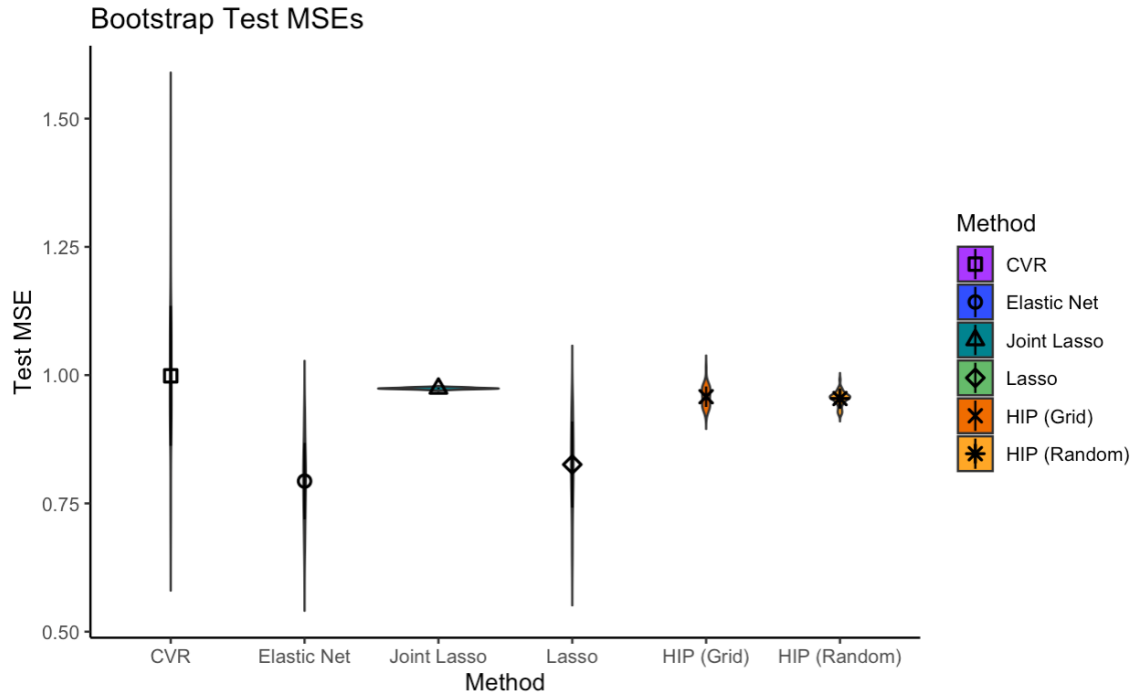


Figure 11: Average overlaid on violin plot of MSEs from fifty bootstrap testing datasets

Table 6: Number of Variables Selected by Each Method

Method	Proteins			Genes		
	Subtype 1	Subtype 2	Common	Subtype 1	Subtype 2	Common
HIP (Random)	34	30	28	66	60	60
HIP (Grid)	30	32	27	58	57	57
Lasso	36	29	2	54	60	1
Elastic Net	36	31	2	54	53	2
CVR	34	31	8	67	66	4
Joint	68	88	11	857	622	76

Table 7: Variables Selected by Random and Grid Searches Using HIP

Data	Subgroup	Random	Grid	Overlap between Random and Grid
Proteins	Subgroup 1 (Males)	34	30	26
	Subgroup 2 (Females)	30	32	25
	Common	28	27	22
Genes	Subgroup 1 (Males)	66	58	40
	Subgroup 2 (Females)	60	57	39
	Common	60	57	39

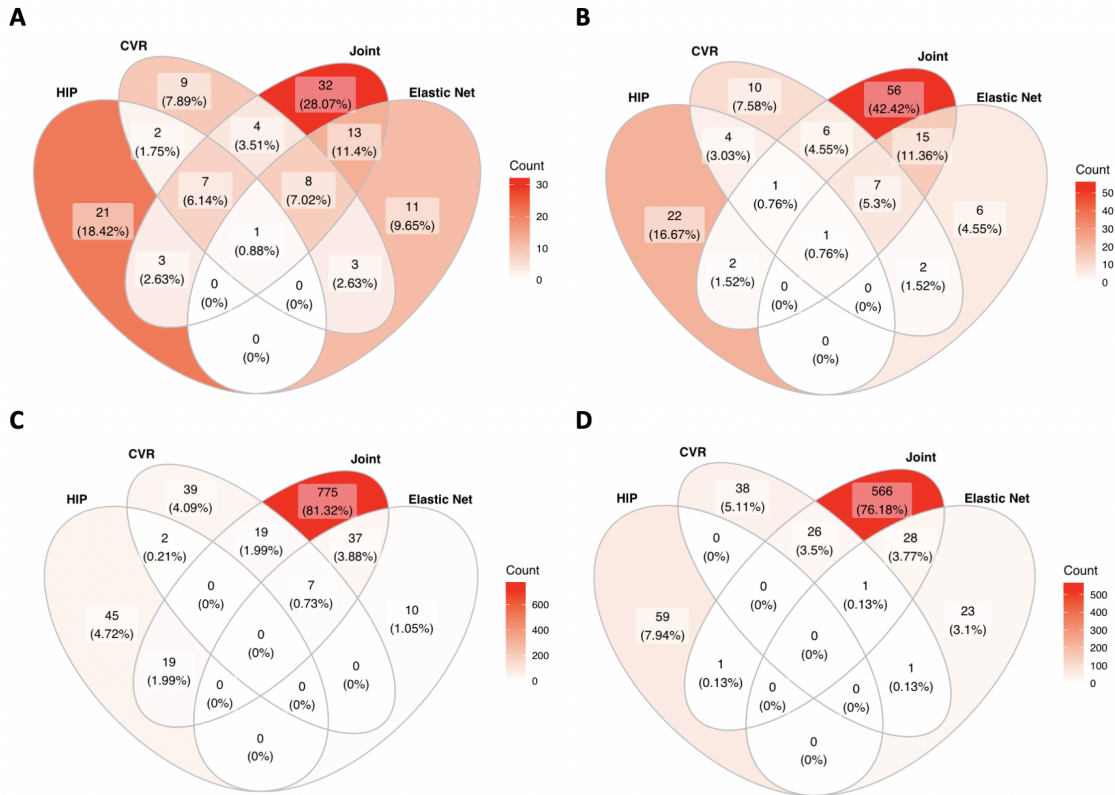


Figure 12: A) Overlap in proteins identified for male subgroup; B) Overlap in proteins identified for female subgroup; C) Overlap in genes identified for male subgroup; D) Overlap in genes identified for female subgroup. HIP used random search for selecting optimal tuning parameters.